



## The Mass of Quasars\*

Yue Shen<sup>1,2†</sup>

<sup>1</sup>*Carnegie Observatories, 813 Santa Barbara Street, Pasadena, CA 91101, USA*

<sup>2</sup>*Hubble Fellow*

Received — ; accepted —

**Abstract.** I review the current status of quasar black hole (BH) mass estimations. Spectroscopic methods have been developed to estimate BH mass in broad line quasars to an accuracy of  $\sim 0.5$  dex. Despite their popularity, significant issues and confusion remain regarding these mass estimators. I provide an in-depth discussion on the merits and caveats of the single-epoch (SE) virial BH mass estimators, and a detailed derivation of the statistical biases of these SE mass estimates resulting from their errors. I show that error-induced sample biases on the order of a factor of several are likely present in the SE mass estimates for flux-limited, statistical quasar samples, and the distribution of SE masses in finite luminosity bins can be narrower than the nominal uncertainty of these mass estimates. I then discuss the latest applications of SE virial masses in quasar studies, including the early growth of supermassive black holes, quasar demography in the mass-luminosity plane, and the evolution of the BH-host scaling relations, with specific emphases on selection effects and sample biases in the SE masses. I conclude that there is a pressing need to understand and deal with the errors in these BH mass estimates, and to improve these BH weighing methods with substantially more and better reverberation mapping data.

*Keywords* : black hole physics — galaxies: active — quasars:general — surveys

### 1. Introduction

Shortly after the discovery of quasars at great cosmological distances (Schmidt 1963), it was realized that the energy required to power these luminous and compact sources must be of gravitational origin rather than from nuclear reaction (e.g., Hoyle & Fowler 1963; Salpeter 1964;

---

\*In this review I use the terms “quasar” and “Active Galactic Nucleus (AGN)” interchangeably to refer to all active supermassive black holes, although traditionally quasars are loosely defined as the luminous ( $L_{\text{bol}} \gtrsim 10^{12} L_{\odot}$ ) subset of AGNs. By default I use quasars and AGNs to refer to unobscured (Type 1), broad-line objects unless otherwise specified.

<sup>†</sup>email: yshen@obs.carnegiescience.edu

Zel'dovich & Novikov 1964; Lynden-Bell 1969). The standard picture now is that mass is accreted onto a supermassive black hole (SMBH) at the center of the galaxy, and the gravitational energy is released during this accretion process to power quasar activity. If the SMBH grows mostly via this accretion process, its mass growth rate is simply:  $\dot{M}_{\text{BH}} = \lambda L_{\text{Edd}}(1 - \epsilon)/(\epsilon c^2)$ , where  $L_{\text{Edd}} = 1M_{\text{BH}} = 1.26 \times 10^{38}(M_{\text{BH}}/M_{\odot}) \text{ erg s}^{-1}$  is the Eddington luminosity of the BH,  $\lambda = L_{\text{bol}}/L_{\text{Edd}}$  is the Eddington ratio, and  $\epsilon$  is the radiative efficiency, i.e., the fraction of accreted rest mass energy converted into radiation. If both  $\lambda$  and  $\epsilon$  are non-evolving, the BH mass increases by one  $e$ -fold on a characteristic timescale  $t_e \equiv \epsilon c^2 / [(1 - \epsilon)\lambda] \approx 4.5 \times 10^8 \frac{\epsilon}{\lambda(1 - \epsilon)} \text{ yr}$ , also known as the Salpeter time or  $e$ -folding time. If quasars do not radiate beyond the Eddington limit  $\lambda = 1$ , the observed luminosity provides a lower-limit on their BH mass (e.g., Zel'dovich & Novikov 1964). The discovery of luminous quasars (with  $L_{\text{bol}} \gtrsim 10^{47} \text{ erg s}^{-1}$ ) at  $z > 6$  (e.g., Fan et al. 2001; Mortlock et al. 2011) then suggests that SMBHs with  $M_{\text{BH}} > 10^9 M_{\odot}$  are already formed in the first billion year after the Big Bang.

In the past two decades or so, there has been tremendous progress in the demographic studies of SMBHs in the nuclei of nearby galaxies (for recent reviews, see, e.g., Kormendy & Richstone 1995; Ferrarese & Ford 2005; Kormendy & Ho 2013). It has come to the consensus that SMBHs with masses of  $\sim 10^5 - 10^{10} M_{\odot}$  are almost ubiquitous at the center of massive galaxies with a significant spheroidal (bulge) component, and also exist in at least some low-mass galaxies. More remarkably, the mass of the nuclear BH is tightly correlated with the properties of the bulge in the local samples (e.g., Gebhardt et al. 2000; Ferrarese & Merritt 2000; Graham et al. 2001; Tremaine et al. 2002; Marconi & Hunt 2003; Aller & Richstone 2007; Gültekin et al. 2009), allowing an estimate of the local SMBH mass function by convolutions with galaxy bulge distribution functions. These BH-bulge scaling relations promoted the notion of BH-galaxy co-evolution, during which the energy release from the accreting SMBH self-regulates its growth, and impacts the formation and evolution of the bulge via feedback processes (e.g., Silk & Rees 1998; King 2003; Di Matteo et al. 2005). Such feedback from active SMBHs (i.e., AGN feedback) has also been invoked in most present-day theoretical modeling of galaxy formation, to bring better agreement with the observed statistics of massive galaxies. However, the significance of AGN feedback and BH-host co-evolution is still under some debate and is an active area of research.

An elegant argument tying the local relic SMBH population to the past active population is the Soltan argument (Soltan 1982): if SMBHs grow mainly through a luminous (or obscured) quasar phase, then the accreted luminosity density of quasars to  $z = 0$ ,  $\rho_{\bullet, \text{acc}}$ , should equal the local relic BH mass density  $\rho_{\bullet}$ :

$$\rho_{\bullet, \text{acc}} = \int_0^{\infty} \frac{dt}{dz} dz \int_0^{\infty} \frac{(1 - \epsilon)L}{\epsilon c^2} \Phi(L, z) dL \approx \rho_{\bullet}, \quad (1)$$

where  $\Phi(L, z)$  is the bolometric luminosity function (LF) per  $L$  interval. Given the observed quasar luminosity function, a reasonably good match between  $\rho_{\bullet, \text{acc}}$  and  $\rho_{\bullet}$  can be achieved if the average radiative efficiency  $\epsilon \sim 0.1$  (e.g., Yu & Tremaine 2002; Shankar et al. 2004; Marconi et al. 2004, also see Salucci et al. 1999; Fabian 1999; Elvis et al. 2002), consistent with the mean  $\epsilon$  value constrained from individual quasars with spectral fitting (e.g., Davis & Laor 2011). The Soltan argument and its variants have been used extensively in recent years to model the growth of

SMBHs with constraints from the demographics of local BH relics and the past AGN population (for a recent review, see Shankar 2009). These exercises are mainly facilitated by the advent of modern large-scale, multiwavelength sky surveys, which have provided large and homogeneous data sets many folds more than what was available twenty years ago, as well as measurements of the abundance and clustering properties of quasars with unprecedented precision.

The growth of SMBHs is among the key science topics in modern galaxy formation studies (for a relatively complete summary of recent progress on this topic, see, e.g., Alexander & Hickox 2012, and references therein). As one of the few fundamental quantities describing a BH, the mass of quasars is of paramount importance to essentially all quasar-related science: the evolution and phenomenology of quasars, accretion physics, the relations and interplays between SMBHs and their host galaxies.

In this review I discuss the current status of quasar BH mass estimations and how these developments can further our understandings of the physics and evolution of SMBHs. I presume the reader has a basic understanding of AGNs and I will skip elaborations on the usual AGN terminologies, which can be found in AGN textbooks (e.g., Peterson 1997; Krolik 1999). This review is mostly pragmatic without going into the detailed and sometimes poorly understood physics behind observations; some further readings can be found in the quoted references.

There are several recent reviews on measuring active and inactive BH masses (e.g., Peterson 2010; Czerny & Nikolajuk 2010; Vestergaard et al. 2011; Marziani & Sulentic 2012), which summarized some general concepts and practical procedures in measuring SMBH masses. While some of the common materials are also covered in the current review for completeness, the scope and focus of this review are different: after an introduction on BH mass measurements in §2, I describe in detail the caveats and statistical biases of the most frequently used BH mass estimators in §3, in light of recent work invoking statistical quasar samples; several applications of these BH mass estimates to quasar studies are discussed in §4, and I conclude this review in §5 with a discussion on future perspectives of improving BH weighing methods. A flat  $\Lambda$ CDM cosmology is adopted throughout this review, with  $\Omega_\Lambda = 0.7$ ,  $\Omega_0 = 0.3$  and  $H_0 = 70 \text{ km s}^{-1} \text{ Mpc}^{-1}$ .

## 2. Methods to Measure Quasar BH Masses

### 2.1 Virial BH Masses: From Reverberation Mapping to Single-Epoch Methods

*Reverberation mapping* The broad emission line regions in AGNs are powered by photoionizations from the central source (e.g., Peterson 1997), an assumption now widely accepted based on observations of correlated broad line and continuum variations. In fact, this photoionization assumption led to the first suggestions (e.g., Bahcall et al. 1972) of lagged broad line responses to continuum variations, where the lag reflects the light travel time from the ionizing source to the broad line region (BLR). In the 1970s there were already reported lag measurements between broad emission line and continuum variations in several local Seyfert nuclei (e.g., Lyutyj & Cherepashchuk 1974). Despite the low data quality that may impact the reliability of

the detection, these studies were among the first attempts to directly measure BLR sizes. This idea was later developed in greater detail by Blandford & McKee (1982), who suggested that by mapping the response function of the broad emission line to continuum variations one can in principle reconstruct the structure and kinematics of the BLR, a technique they coined “reverberation mapping” (RM). Today RM has become a practical and powerful tool to study BLRs (see reviews by, e.g., Peterson 1993; Netzer & Peterson 1997; Horne et al. 2004), whose spatial extent ( $\sim$  sub-pc) is too small to be resolved by current instrumentation. There are now several dozens of AGNs and quasars (most are at  $z < 0.3$ ) with average lag measurements (e.g., Kaspi et al. 2000; Peterson et al. 2004; Bentz et al. 2009b), although only a handful of them have decent velocity-resolved delay maps (e.g., Denney et al. 2009a; Bentz et al. 2010; Grier et al. 2013) to utilize the full power of RM.

RM lag measurements provide an estimate of the typical size of the BLR. If we further assume that the BLR is virialized and the motion of the emitting clouds is dominated by the gravitational field of the central BH, then the mass of the BH is determined by (e.g., Ho 1999; Wandel et al. 1999):

$$M_{\text{RM}} = \frac{V_{\text{vir}}^2 R}{G} = f \frac{W^2 R}{G}, \quad (2)$$

where  $V_{\text{vir}}$  is the virial velocity and  $R$  is the BLR size. In practice we use the width of the broad line,  $W$ , as an indicator of the virial velocity, assuming that the broad line is Doppler broadened by the virial motion of the emitting gas. The product  $W^2 R/G$  is called the virial product. There are two commonly used line width definitions, the “full-width-at-half-maximum” (FWHM), and the line dispersion  $\sigma_{\text{line}}$  (i.e., the second moment of the line, Peterson et al. 2004). The pros and cons of both definitions will be discussed later. In computing the RM BH masses, both line widths are measured from the rms spectra from the monitoring period, thus only the variable part of the line contributes to the line width calculation.

To account for our ignorance of the structure and geometry of the BLR which determine the relation between the virial velocity and the line-of-sight (LOS) velocity inferred from  $W$ , we have introduced a virial coefficient (or geometrical factor),  $f^1$ , in Eqn. (2). This is a big simplification, because the BLR structure and viewing angle determine the entire line profile, and the line width, being only one characteristic of the line profile, can not fully describe the underlying kinematic structure. Similarly it is an approximation to describe the BLR with a single radius  $R$ . Nevertheless, given the difficulties and ambiguities of modeling the line profile directly, Eqn. (2) involving line widths and  $f$  is used almost universally. For BLR clouds in randomly orientated orbits, an often quoted value is  $f \approx 3/4$  (3) if  $W = \text{FWHM}$  ( $\sigma_{\text{line}}$ ) (Netzer 1990), although such a  $f$  value is derived under some simplifications and approximations and is not a rigorous analytic result. In practice, the value of  $f$  is now empirically determined by requiring that the derived RM masses are consistent with those predicted from the BH mass-bulge stellar velocity dispersion ( $M_{\text{BH}} - \sigma_*$ ) relation of local inactive galaxies (e.g., Onken et al. 2004):  $f \approx 1.4$  (5.5) for  $W = \text{FWHM}$  ( $\sigma_{\text{line}}$ ). This  $f$  value is of course then the averaged value

---

<sup>1</sup>Some studies define the virial coefficient differently, i.e.,  $V_{\text{vir}} \equiv fW$  (e.g., McLure & Jarvis 2002; Decarli et al. 2008a).

for the subset of RM AGNs with bulge stellar velocity dispersion measurements. The uncertainty in  $f$  and the simplification of it as a single constant remain one of the major uncertainties in RM mass determinations, as further discussed in §3.1.2.

The uncertainty of the RM masses is typically a factor of a few, or  $\sim 0.4 - 0.5$  dex (e.g., Peterson 2010), based on comparisons between RM masses and predictions from the  $M_{\text{BH}} - \sigma_*$  relation, and accounting for other potential systematics.

*The  $R - L$  relation* Perhaps the most remarkable finding of RM observations is a tight correlation between the measured BLR size and the adjacent optical continuum luminosity  $L_{\text{opt}}$  (usually measured at restframe 5100 Å),  $R \propto L^\alpha$ , over  $\sim 4$  orders of magnitude in luminosity. This is known as the BLR size-luminosity relation, or the  $R - L$  relation (e.g., Kaspi et al. 2000, 2005; Bentz et al. 2009a). To first order all broad line quasars have similar spectral energy distributions (SEDs) from X-ray to optical<sup>2</sup>, so  $L_{\text{opt}}$  is proportional to the ionizing continuum  $L_{\text{ion}}$ . The ionization parameter in a photoionized medium is  $U = Q(H)/(4\pi r^2 c n_e)$ , where  $Q(H) \propto L$  is the number of ionizing photons from the central source per second,  $c$  is the speed of light, and  $n_e$  is electron density. Thus a slope of  $\alpha = 0.5$  in the  $R - L$  relation is expected, if  $U$  and the electron density are more or less constant in BLRs. Alternatively, a slope of  $\alpha = 0.5$  is also predicted if the BLR size is set by dust sublimation (e.g., Netzer & Laor 1993).

Early RM work reported a slope of  $\alpha \sim 0.7$  (e.g., Kaspi et al. 2000). Later work which carefully accounted for host starlight contamination to  $L_{\text{opt}}$  reported  $\alpha \approx 0.5$  (e.g., Bentz et al. 2009a), closer to naive expectations from photoionization. The intrinsic scatter of the  $R - L$  relation is estimated to be  $\sim 0.15$  dex ( $\sim 0.11$  dex with the best quality RM data, Peterson 2010). The latest version of the  $R - L$  relation based on H $\beta$  RM measurements is (Bentz et al. 2009a):

$$\log \frac{R}{\text{light days}} = -21.3 + 0.519 \log \frac{\lambda L_\lambda(5100\text{\AA})}{\text{erg s}^{-1}}. \quad (3)$$

The tightness of the  $R - L$  relation has led to suggestions to use this relation as an absolute luminosity indicator to use quasars as a cosmology probe (e.g., Watson et al. 2011; Czerny et al. 2012), although RM measurements of BLR sizes and quantification of the  $R - L$  relation beyond  $z \sim 0.3$  are yet to come (e.g., Kaspi et al. 2007).

*Single-epoch (SE) virial BH mass estimators* The observed  $R - L$  relation provides a much less expensive way to estimate the size of the BLR based on the luminosity of the quasar. Subsequently this relation has been used to develop the so-called “single-epoch virial black hole mass estimators”<sup>3</sup> (SE virial masses or SE masses in short hereafter): one estimates the BLR size from

<sup>2</sup>It is also important to recognize that AGN SEDs can vary significantly from object to object, and some of these variances in SED must introduce certain scatter in the observed  $R - L$  relation based on measurable continuum instead of the ionizing continuum, and may cause systematic changes of BLR structure with SED properties (which might affect the virial coefficient  $f$ ).

<sup>3</sup>Such methods are also known as BH mass scaling methods (e.g., Vestergaard et al. 2011). Occasionally, this method is referred to as the “photoionization method” (e.g., Peterson 2011; Salviander & Shields 2012). This may be a little

the measured quasar luminosity using the  $R - L$  relation, and the width of the broad emission line, which are then combined to give an estimate of the BH mass using calibration coefficients determined from the sample of AGNs with RM mass estimates. Specifically, these estimators take the form:

$$\log\left(\frac{M_{\text{SE}}}{M_{\odot}}\right) = a + b \log\left(\frac{L}{10^{44} \text{ erg s}^{-1}}\right) + c \log\left(\frac{W}{\text{km s}^{-1}}\right), \quad (4)$$

where  $L$  and  $W$  are the quasar continuum (or line) luminosity and width for the specific line, and coefficients  $a$ ,  $b$  and  $c$  are calibrated against RM AGNs. In Eqn. (4), the coefficient on line width is usually taken to be  $c = 2$ , as expected from viral motion. Other values of  $c$  are suggested, however, depending on the definition of line width, and will be discussed further in §3. Based on the general similarity of quasar SEDs (both continuum and line strength), different luminosities have been used, including continuum luminosities in X-ray, restframe UV and optical, as well as line luminosities, in various versions of these single-epoch virial estimators (e.g., Vestergaard 2002; McLure & Jarvis 2002; McLure & Dunlop 2004; Wu et al. 2004; Greene & Ho 2005; Vestergaard & Peterson 2006; Kollmeier et al. 2006; Onken & Kollmeier 2008; Wang et al. 2009; Vestergaard & Osmer 2009; Greene et al. 2010b; Rafiee & Hall 2011b; Shen et al. 2011; Shen & Liu 2012; Trakhtenbrot & Netzer 2012). In general continuum luminosities are preferred over line luminosities given their tighter correlations with BLR size, but in some cases line luminosities are preferred where the continuum may be significantly contaminated by host starlight (e.g., Greene & Ho 2005), or by the nonthermal emission from a jet in radio-loud objects (e.g., Wu et al. 2004). As for the choice of line width, both FWHM and line dispersion ( $\sigma_{\text{line}}$ ) are utilized in these calibrations.

The uncertainty of these various single-epoch virial estimators can be inferred from the residuals in the calibrations against the RM masses, and is estimated to be on the order of  $\sim 0.5$  dex (e.g., McLure & Jarvis 2002; Vestergaard & Peterson 2006). This is similar to the uncertainty of RM masses, and can hardly be smaller since this method is rooted in the RM technique. Reasons and consequences of such substantial mass uncertainties will be elaborated in §3. From now on I will refer to RM and SE masses collectively as virial BH masses.

The virial estimators (RM and SE) currently are the best method in estimating quasar BH masses. Therefore after a brief discussion on alternative methods (§2.2), I will focus on these virial estimators in the rest of the review.

## 2.2 Other Methods to Estimate Quasar BH Masses

There are several other methods to estimate the mass of quasars. They are much less popular than the RM method and its extension, the SE virial method. Nevertheless there is certain merit in

---

ambiguous, since in practice this empirical method is based on RM results rather than photoionization calculations, even though the observed  $R - L$  relation is consistent with naive photoionization predictions. The “photoionization method” better refers to those that estimate the BLR size using photoionization arguments (see §2.2).

further developing some of these methods, for instance, to provide complementary mass estimates and consistency checks. Therefore I give a brief discussion on these alternative methods.

*Photoionization method* Historically Dibai was the first to systematically measure BH masses for quasar samples since the 1970s (e.g., Dibai 1977, 1980, 1984). Adopting Woltjer’s postulation that the BLR gas is in virial equilibrium in the gravitational potential of the central BH (Woltjer 1959), Dibai used Eqn. (2) to estimate the BH mass, where the width of the line is used to indicate the virial velocity. To estimate the BLR size  $R$ , Dibai used the photoionization argument:

$$L(\text{H}\beta) = \frac{4\pi}{3} R^3 j(n_e T_e) \epsilon_V, \quad (5)$$

where  $L(\text{H}\beta)$  is the luminosity of the  $\text{H}\beta$  line,  $j(n_e T_e)$  is the volume emissivity in the  $\text{H}\beta$  line from photoionized gas, and  $\epsilon_V$  is the volume filling factor of BLR clouds. Adopting constant values of  $n_e \approx 10^9 \text{ cm}^{-3}$ ,  $T_e \approx 10^4 \text{ K}$  and  $\epsilon_V \approx 10^{-3}$ , Dibai estimated BH masses for more than  $\sim 70$  nearby Seyfert 1 galaxies and quasars, and made the first plot of the distribution of AGNs in the mass-luminosity plane. Technically speaking, Dibai’s method is also a single-epoch method, and it has an effective  $R-L$  relation of  $R \propto L(\text{H}\beta)^{1/3}$ , shallower than the observed  $R-L$  relation. Despite the simplifications in Dibai’s approach (sometimes unphysical), many of his BH mass estimates of local AGNs are consistent with today’s RM masses to within 0.3 dex (e.g., Bochkarev & Gaskell 2009). Dibai’s method also motivated some later quasar BH mass estimations based on the same argument. For example, Wandel & Yahil (1985) used the same method with modifications to the volume filling factor, and derived a radius-luminosity relation  $R \propto L(\text{H}\beta)^{1/2}$ .

Along a completely independent path, photoionization arguments based on the ionization parameter  $U$  were used to estimate the BLR size (e.g., Netzer 1990; Wandel et al. 1999), building on earlier development of photoionization equilibrium theory in the 1970s (e.g., Davidson 1972; Davidson & Netzer 1979). This approach emphasizes more on the role of the ionization continuum, and provides an intuitive understanding of the observed  $R-L$  relation. But just as Dibai’s method, all these photoionization-based methods require assumptions or indirect constraints on the physical conditions of the BLR gas (such as density, covering factor, etc) to infer the BLR size, therefore today they are not as popular as the more empirical, but more accurate RM-based methods discussed in §2.1.

*Accretion disk model fitting (SED fitting)* Another method to infer the mass of the BH is by fitting the SED of quasars. The development of accretion disk theory over the last four decades (for a recent review, see, e.g., Abramowicz & Fragile 2013) has enabled predictions of the emitting continuum spectrum of accreting BHs. By fitting the observed quasar continuum SED, one can constrain the model parameters (such as BH mass, accretion rate, BH spin, inclination) with adequate accretion disk models. Many studies have used this SED fitting method to infer BH masses in AGNs (e.g., Malkan 1983; Sun & Malkan 1989; Wandel & Petrosian 1988; Laor 1990; Rokaki et al. 1992; Tripp et al. 1994; Ghisellini et al. 2010; Calderone et al. 2012), usually assuming a standard thin accretion disk model (Shakura & Sunyaev 1973). One main concern here is that standard accretion disk models, while can successfully produce broad-band features (such as the “big blue bump”, e.g., Shields 1978), do not yet have the capability to fully explain the AGN SED (e.g., Koratkar & Blaes 1999; Lawrence 2012), and the resulting BH mass constraints

may be sensitive to these deviations from standard accretion disk models. Given that there are parameter degeneracies and model assumptions/simplifications in the SED fitting procedure and the requirement for good multiwavelength coverage in UV-optical (where most of the disk emission comes from), this method generally cannot provide an accuracy of better than a factor of  $\sim$  five in BH mass estimates at the moment (e.g., Laor 1990; Calderone et al. 2012). But it would be interesting to compare this method with the virial methods (§2.1) for larger samples.

*Micro lensing in gravitationally lensed quasars – alternative routes to BLR sizes* Since resolving the BLRs requires  $\mu$ s to tens of  $\mu$ s angular resolution, RM will remain the primary method to measure the size of BLR in the next decade or two. Another indirect method to measure BLR size is via microlensing in gravitationally lensed quasars. The Einstein radius in the source (quasar) plane of a point-mass lens with mass  $M$  is  $r_E = \sqrt{4GM D_s D_{LS} / (D_L c^2)}$ , where  $D_s$ ,  $D_L$  and  $D_{LS}$  are the angular diameter distances to the source, to the lens, and from the lens to the source. For typical values  $z_L = 0.5$  and  $z_S = 2$  we have  $r_E \approx 0.01 \sqrt{M/M_\odot}$  pc, corresponding to an angular scale  $\theta_E = r_E/D_S \approx \sqrt{M/M_\odot} \mu$ as. This scale is comparable to the size of the BLR and accretion disk. Due to the relative transverse motion between the lens and source, large magnification can happen on short time scales ( $t_{\text{cross}} = r_{\text{source}}/v_\perp$ ) during caustic-crossing in the source plane (for a primer on gravitational lensing, see, e.g., Schneider et al. 1992). Since the continuum emission (from the inner accretion disk) and BLR emission have different spatial scales<sup>4</sup>, microlensing will cause differential variability for the continuum and different broad lines, which can be used to constrain the size (and geometry) of the emitting regions, such as the accretion disk and the BLR (e.g., Irwin et al. 1989; Lewis et al. 1998; Popović et al. 2001; Richards et al. 2004a; Morgan et al. 2010; Dai et al. 2010; Mosquera & Kochanek 2011; Sluse et al. 2011, 2012; Guerras et al. 2013). In particular, the latest study by Guerras et al. (2013) found a  $R - L$  relation based on microlensing BLR sizes, which is in reasonably good agreement with that based on RM. This technique is primarily applied to quasars that are already strongly lensed (with multiple images) for which the microlensing probability by stars/compact objects in the foreground lens galaxy is high, and the time delays between different images are known. The latter is important to rule out variability due to intrinsic AGN variability, which will often complicate the microlensing interpretation.

*Direct dynamical BH masses* Although observationally challenging (given the overwhelming AGN continuum that dilutes the stellar absorption features and nongravitational forces on gas dynamics in the nucleus), there have been several attempts to get direct dynamical measurements of BH masses in Type 1 AGNs, using spatially resolved stellar kinematics (e.g., Davies et al. 2006; Onken et al. 2007) or gas kinematics (e.g., Hicks & Malkan 2008) down to the sphere of influence,  $R_{\text{SI}} = GM_{\text{BH}}/\sigma_*^2$ , of the BH. The number of AGNs with reliable dynamical BH mass measurements is still small, and it would be important to obtain more dynamical mass measurements of AGNs to provide critical consistency checks on virial BH masses.

---

<sup>4</sup>The BLR and the accretion disk are probably not disjointed, i.e., some portion of the BLR gas could originate from the outer part of the accretion disk or from a wind launched from the disk, and high-ionization lines could have different origins from low-ionization lines, as in some models (e.g., Collin-Souffrin et al. 1988; Elvis 2000; Risaliti & Elvis 2010).



*Other indirect methods* These methods use correlations between BH mass and other measurable quantities, calibrated with known BH masses, to infer the BH mass in quasars. By virtue they can be applied to non-broad-line quasars as well, if the required quantity is measurable, but caution should be paid to possible systematics of each method. These correlations include the well-known BH-host scaling relations found for local inactive galaxies. For instance, the  $M_{\text{BH}} - \sigma_*$  relation in local inactive galaxies is used to predict BH masses in local RM AGNs with  $\sigma_*$  measurements (see §3.1.2). Another example is the observed anti-correlations between BH mass (estimated with other methods) and X-ray variability properties of AGNs, such as the break frequency in the power spectral densities (PSDs) of X-ray light curves or variability amplitude (e.g., Papadakis 2004; O’Neil et al. 2005; McHardy et al. 2006; Zhou et al. 2010), which have the potential to provide independent BH mass estimates to within a factor of a few to the RM masses. The reliability and systematics of the X-ray variability method, however, are yet to be explored with larger AGN samples with known BH masses.

### 3. Caveats, Uncertainties, and Biases of Virial BH Masses

#### 3.1 Physical Concerns

##### 3.1.1 *The virial assumption*

There are evidence supporting the virial assumption in RM in at least several AGNs (e.g., Peterson & Wandel 1999, 2000; Onken & Peterson 2002; Kollatschny 2003). For these objects RM lags have been successfully measured for multiple lines with different ionization potentials (such as  $\text{H}\beta$ ,  $\text{CIV}$ ,  $\text{HeII}$ ) and line widths, which are supposed to arise at different distances, as in a stratified BLR for different lines. The measured lags and line widths of these different lines fall close to the expected virial relation  $W \propto R^{-1/2}$ , although such a velocity-radius scaling does not necessarily rule out other BLR models where the dynamics is not dominated by the gravity of the central BH (e.g., see discussions in Krolik 2001). A more convincing argument is based on velocity-resolved RM, where certain dynamical models (such as outflows) can be ruled out based on the difference (or lack thereof) in the lags from the blue and red parts of the line (e.g., Gaskell 1988). On the other hand, non-virial motions (such as infall and/or outflows) may indeed be present in some BLRs, as inferred from recent velocity-resolved RM in a handful of AGNs (e.g., Denney et al. 2009a; Bentz et al. 2010; Grier et al. 2013). Fortunately, even if the BLR is in a non-virial state, one might still expect that the velocity of the BLR clouds (as measured through the line width) does not deviate much from the virial velocity. Thus using Eqn. (2) does not introduce a large bias, and in principle this detail is accounted for by the virial coefficient  $f$  in individual sources.

A further test of the virial assumption on the single-epoch virial estimators is to see if the line width varies in accordance to the changes in luminosity for the same object. The picture here is that when luminosity increases (decreases) the BLR expands (shrinks), and the line width should decrease (increase), given enough response time. This test is important, because if the line width does not change accordingly to luminosity changes, the SE mass will change for the

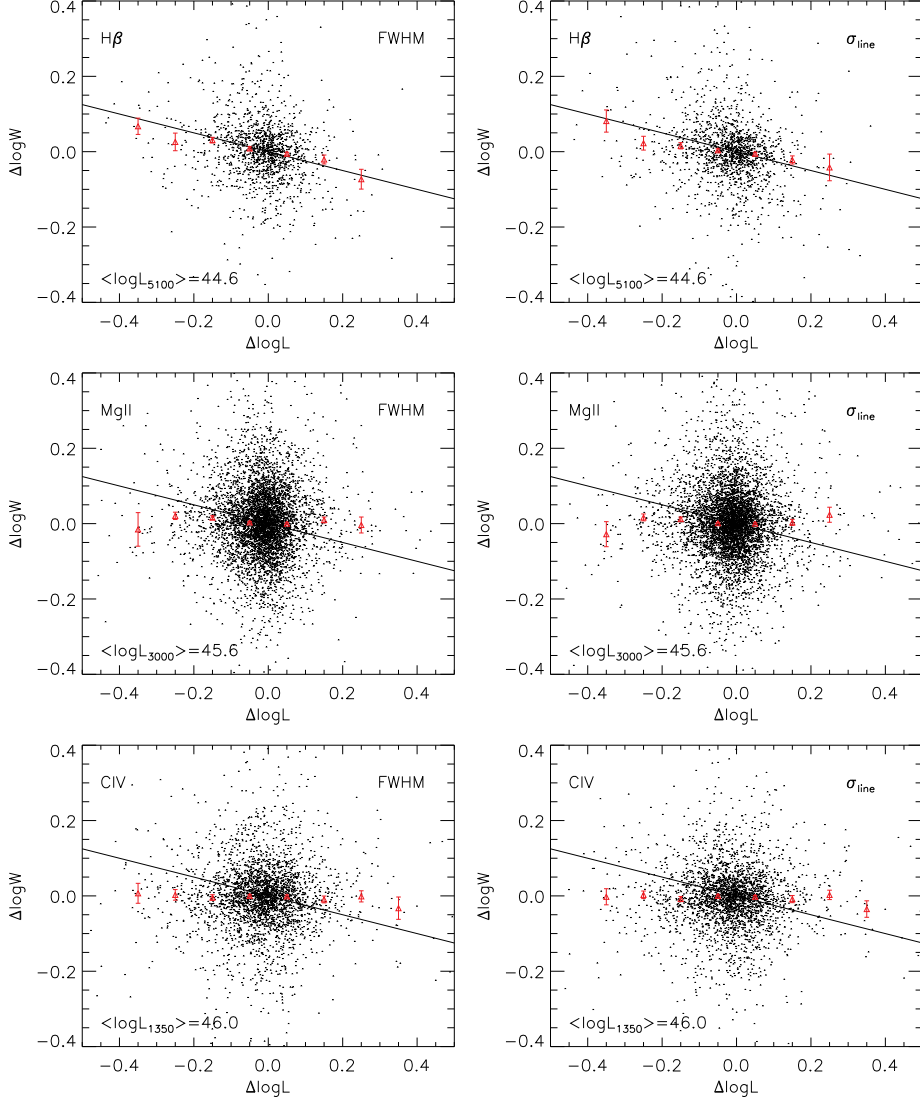


**Figure 1.** A test of the virial assumption using two-epoch spectroscopy from SDSS for  $H\beta$  (upper),  $Mg\ II$  (middle) and  $CIV$  (bottom). Plotted here are the changes in line width as a function of changes in continuum luminosity ( $L_{5100}$ ,  $L_{3000}$ , and  $L_{1350}$  for  $H\beta$ ,  $Mg\ II$ , and  $CIV$ , respectively) between the two epochs. The left column is for FWHM and the right column is for  $\sigma_{line}$ . The dots are for all objects with measurement  $S/N > 3$  at both epochs for both  $L$  and  $W$  (not for  $\Delta \log L$  and  $\Delta \log W$ ). These objects tend to cluster around zero values because the typical continuum and line variabilities of SDSS quasars are small. The red triangles are the median values in each  $\Delta \log L$  bin, where the error bars indicate the uncertainty in the mean. A perfect virial relation would imply  $\Delta \log W = -0.25 \Delta \log L$ , as indicated by the solid line in each panel. Note that I have neglected the chromatic nature of quasar variability, which would predict an even steeper relation between  $\Delta \log W$  and  $\Delta \log L$  (see §3.1.1 for details). The low-redshift  $z \lesssim 0.7$  SDSS quasars with median luminosity  $\langle \log(L_{5100}/\text{erg s}^{-1}) \rangle = 10^{44.6}$  show the expected virial relation between  $\Delta \log L$  and  $\Delta \log W$ , which is not the case for the high-luminosity SDSS quasars at  $z > 0.7$  based on  $Mg\ II$  or  $CIV$ .

same object, introducing a luminosity-dependent bias in the mass estimates (see §3.3.2). This test is challenging in practice, given the limited dynamic range in continuum variations and the presence of measurement errors. Nevertheless, in several AGNs with high-quality RM data, such anti-correlated variations of line width and BLR size (or continuum luminosity) have been seen (e.g., Peterson et al. 2004; Park et al. 2012b), once the lag between continuum and line variations is taken into account. While this lends some further support for RM and SE virial estimators, it should be noted that: 1) not all RM AGNs show this expected behavior, given insufficient data quality; 2) it makes a difference which line width measurements (i.e., FWHM vs  $\sigma$ , rms vs mean spectra) and which BLR size estimates (i.e.,  $\tau$  vs continuum luminosity) are used.

It is also not clear if the above results based on a few RM AGNs apply to the general quasar population. Fig. 1 shows a test of the co-variation of line width and continuum luminosity using thousands of SDSS quasars with spectra at two epochs (She, Shen, et al., in prep). While for the majority of these quasars the two epochs do not span a large dynamic range in luminosity, the large number of objects provide good statistical constraints on the average trend. In Fig. 1 the black dots are measurements for individual objects, and they cluster near the center because most quasars do not vary much between the two epochs. The measurement uncertainties on  $\Delta \log L$  and  $\Delta \log W$  are large, so I bin the results in  $\Delta \log L$  bins and plot the medians and uncertainties in the median in each bin in red triangles. The measurement uncertainties in  $\Delta \log L$  and  $\Delta \log W$  are comparable for all three lines, but only for the low-luminosity and low- $z$  ( $z \lesssim 0.7$ ) H $\beta$  sample is the median relation consistent with the virial relation (the solid lines in Fig. 1). For the other samples at  $z > 0.7$  based on Mg II and C IV, the line width does not seem to respond to luminosity changes as expected from the virial relation. This difference could be a luminosity effect, but more detailed analyses are needed (She, Shen, et al., in prep).

Another important point to make is that there is a well known fact that quasar spectra get harder (bluer) as they get brighter (e.g., Vanden Berk et al. 2004, and references therein). This means that the variability amplitude in the ionizing continuum should be larger than that at longer wavelengths (i.e., the observed continuum). Thus we should see a somewhat steeper slope in the line width change versus the (observed) continuum luminosity change plot for a single object (e.g., Peterson et al. 2002). This, however, would be in an even larger disagreement with the trends we see in Fig. 1.

### 3.1.2 The virial coefficient $f$

To relate the observed broad line width to the underlying virial velocity (e.g., Eqn. 2) requires the knowledge of the (emissivity weighted) geometry and kinematics of the BLR. In principle RM can provide such information, and determine the value of  $f$  from first principles. Unfortunately the current RM data are still not good enough for such purposes in general, although in a few cases alternative approaches have been invented lately to account for the effect of  $f$  in directly modeling the RM data using dynamical BLR models (e.g., Brewer et al. 2011; Pancoast et al. 2012). Early studies made assumptions about the geometry and structure of the BLR in deriving RM masses (e.g., Netzer 1990; Wandel et al. 1999; Kaspi et al. 2000) or SE virial masses

(e.g., McLure & Dunlop 2004). Now the average value of  $f$  is mostly determined empirically by requiring that the RM masses are consistent with those predicted from the  $M_{\text{BH}} - \sigma_*$  relation of local inactive galaxies. Such an exercise was first done by Onken et al. (2004), who used 16 local AGNs with both RM measurements and stellar velocity dispersion measurements to derive  $\langle f \rangle \approx 1.4$  if FWHM is used, or  $\langle f \rangle \approx 5.5$  if  $\sigma_{\text{line}}$  is used. Later this was repeated with new RM data (e.g., Woo et al. 2010), who derived a similar value of  $\langle f \rangle \approx 5.2$  (using  $\sigma_{\text{line}}$ ).

However, in recent years it has become evident that the scaling relations between BH mass and bulge properties are not as simple as we thought: it appears that different types of galaxies follow somewhat different scaling relations, and the scatter seems to increase towards less massive systems (e.g., Hu 2008; Greene et al. 2008; Graham 2008; Graham & Li 2009; Hu 2009; Gültekin et al. 2009; Greene et al. 2010b; McConnell & Ma 2012, and references therein). Therefore, depending on the choice of the specific form of the  $M_{\text{BH}} - \sigma_*$  relation used and the types of galaxies hosting RM AGNs in the calibration, the derived average  $f$  value could vary significantly. For instance, Graham et al. (2011) derived a  $\langle f \rangle$  value that is only half of the values derived by Onken et al. (2004) and Woo et al. (2010). Park et al. (2012b) performed a detailed investigation on the effects of different regression methods and sample selection in determining the  $M_{\text{BH}} - \sigma_*$  relation and in turn the  $\langle f \rangle$  value, and concluded that the latter is the primary cause for the discrepancy in the reported  $\langle f \rangle$  values. Given the small sample sizes of RM AGNs with host property measurements and the uncertainties in the BH-host scaling relations in inactive galaxies, the uncertainty of  $\langle f \rangle$  is still  $\sim$  a factor of 2 or more, and will remain one of the main obstacles to estimate accurate RM (or SE) BH masses in terms of the overall normalization. One may also expect that the actual  $f$  value is different in individual sources, either from the diversity in BLR structure or from orientation effects (since the line width only reflects the line-of-sight velocity, see §3.1.6). Thus using a constant  $f$  value in these RM masses and SE virial estimators introduces additional scatter in these mass estimates.

Perhaps a more serious concern is the assumption that the BH-host scaling relations are the same in active and inactive galaxies. While there is a clear correlation between bulge properties and the RM masses in RM AGNs (e.g., Bentz et al. 2009c), it could be offset from that for inactive galaxies if the actual  $\langle f \rangle$  value is different. Such a scenario is plausible if the BH growth and host bulge formation are not always synchronized. The only way to tackle this problem is to infer  $f$  from directly constrained BLR geometry/kinematics with exquisite velocity-resolved RM data that map the line response (transfer function) in detail, and this must be done for a large number of AGNs to explore its diversity.

### 3.1.3 FWHM versus line dispersion

Both FWHM and  $\sigma_{\text{line}}$  are commonly used in SE virial mass estimates as the proxy for the virial velocity (when combined with the virial coefficient  $f$ ). Both definitions have advantages and disadvantages. FWHM is a quantity that is easier to measure, less susceptible to noise in the wings and treatments of line blending than  $\sigma_{\text{line}}$ , while  $\sigma_{\text{line}}$  is less sensitive to the treatment of narrow line removal and peculiar line profiles. Overall FWHM is preferred over  $\sigma_{\text{line}}$  in terms of

easiness of the measurement and repeatability. As  $\sigma_{\text{line}}$  measurements depend sensitively on data quality and different methods used (e.g., Denney et al. 2009b; Rafiee & Hall 2011a,b; Assef et al. 2011), the SE virial masses (e.g., Eqn. 4) based on  $\sigma_{\text{line}}$  could differ significantly for the same objects.

Physically one may argue  $\sigma_{\text{line}}$  is more trustworthy to use than FWHM, although the evidence to date is only suggestive. Collin et al. (2006) compared the virial products based on both  $\sigma_{\text{line}}$  and FWHM with those expected from the  $M_{\text{BH}} - \sigma_*$  relation, for 14 RM AGNs. All their line width measurements were based on the rms or mean spectra of the RM AGNs. They found that the average scale factor (i.e., the virial coefficient  $f$ ) between virial products to the  $M_{\text{BH}} - \sigma_*$  masses depends on the shape of the line if FWHM is used, while it is more or less constant if  $\sigma_{\text{line}}$  is used. Based on this, they argue that  $\sigma_{\text{line}}$  is a better surrogate to use in estimating RM masses. Additionally,  $\sigma_{\text{line}}$  measured in rms spectra seems to follow the expected virial relation better than FWHM in some RM AGNs (e.g., Peterson et al. 2004), although such evidence is circumstantial.

It is important to note that for a given line, the ratio of FWHM to  $\sigma_{\text{line}}$  is not necessarily a constant (e.g., Collin et al. 2006; Peterson 2011, but cf., Decarli et al. 2008a), while a Gaussian line profile leads to  $\text{FWHM}/\sigma_{\text{line}} \approx 2.35$ . For  $\text{H}\beta$ ,  $\text{FWHM}/\sigma_{\text{line}}$  seems to increase when the line width increases. This might be related to the Populations A and B sequences developed by Sulentic and collaborators (Sulentic et al. 2000a), which is an extension of earlier work on the correlation space of AGNs (the so-called “eigenvector 1”, e.g., Boroson & Green 1992; Wang et al. 1996). A direct consequence is that there will be systematic differences in  $M_{\text{SE}}$  whether FWHM or  $\sigma_{\text{line}}$  is used for the same set of quasars, especially for objects with extreme line widths. In general a “tilt” between the FWHM and  $\sigma_{\text{line}}$ -based virial masses is expected (e.g., Rafiee & Hall 2011a,b). Currently directly measuring  $\sigma_{\text{line}}$  from single-epoch spectra is much more ambiguous and methodology-dependent than measuring FWHM. If one accepts that  $\sigma_{\text{line}}$  is a more robust virial velocity indicator, it is possible to convert the measured FWHM to  $\sigma_{\text{line}}$  using the relation found for high S/N data (e.g., Collin et al. 2006), or empirically determine the dependence of SE mass on FWHM (i.e., coefficient  $c$  in Eqn. 4) using RM masses as calibrators (e.g., Wang et al. 2009), which generally leads to values of  $c < 2$ .

The choice of line width indicators is still an open issue. It will be important to revisit the arguments in, e.g., Collin et al. (2006), using not only more but also better-quality RM data, as well as to investigate the behaviors of FWHM and  $\sigma_{\text{line}}$  (and perhaps alternative line width measures) for large quasar samples.

### 3.1.4 Broad line profiles

As briefly mentioned in §2.1, part of the reason that we are struggling with  $f$  and line width definitions is because of the simplifications of a single BLR size and using only one line profile characteristic to infer the underlying BLR velocity structure. If we have a decent understanding of the BLR dynamics and structure (geometry, kinematics, emissivity, ionization, etc.), then in principle we can solve the inverse problem of inferring the virial velocity from the broad line

profile. Unfortunately, the detailed BLR properties are yet to be probed with velocity-resolved reverberation maps, and the solution of this inverse problem may not be unique (e.g., different BLR dynamics and structure may produce similar line profiles).

Nevertheless, there have been efforts to model the observed broad line profiles with simple BLR models. The best known example is the disk-emitter model (e.g., Chen et al. 1989; Eracleous & Halpern 1994; Eracleous et al. 1995), where a Keplerian disk with a turbulent broadening component is used to model the double-peaked broad line profile seen in  $\sim 10 - 15\%$  radio-loud quasars (and several percent of radio-quiet quasars). The line profile then can place constraints on certain geometrical parameters, such as the inclination of the disk, thus has relevance in the  $f$  value for individual objects (e.g., La Mura et al. 2009). Another example is using simple kinematic BLR models to explain the trend of the line shape parameter  $\text{FWHM}/\sigma_{\text{line}}$  as a function of line width (e.g., Kollatschny & Zetzl 2011, 2013), as mentioned earlier in §3.1.3. These authors found that a turbulent component broadened by a rotation component can explain the observed trend of line shape parameter, and their model provides conversions between the observed line width and the underlying virial (rotational) velocity. More complicated BLR models can be built (e.g., Goad et al. 2012), which has the potential to underpin a physical connection between the BLR structure and the observed broad line characteristics. While all these exercises are worth further investigations, it is important to build self-consistent models that are also verified with velocity-resolved RM.

### 3.1.5 *Effects of host starlight and dust reddening*

The luminosity that enters the  $R - L$  relation and the SE mass estimators (Eqn. 4) refers to the AGN luminosity. At low AGN luminosities, the contamination from host starlight to the  $5100\text{\AA}$  luminosity can be significant. This motivated the alternative uses of Balmer line luminosities in Eqn. (4) (e.g., Greene & Ho 2005). Using line luminosity is also preferred for radio-loud objects where the continuum may be severely contaminated by the nonthermal emission from the jet (e.g., Wu et al. 2004). Bentz et al. (2006) and Bentz et al. (2009a) showed that properly accounting for the host starlight contamination at optical luminosities in RM AGNs leads to a slope in the  $R - L$  relation that is closer to the naive expectation from photoionization. Similarly, using host-corrected  $L_{5100}$  can lead to reduced scatter in the  $H\beta - L_{5100}$  SE calibration against RM AGNs (e.g., Shen & Kelly 2012).

The average contribution of host starlight to  $L_{5100}$  has been quantified by Shen et al. (2011), using low-redshift SDSS quasars. They found that significant host contamination ( $\geq 20\%$ ) is present for  $\log L_{5100, \text{total}} < 10^{44.5} \text{ erg s}^{-1}$ , and provided an empirical correction for this average contamination. Variations in host contribution could be substantial for individual objects though.

For UV luminosities ( $L_{3000}$ ,  $L_{1350}$  or  $L_{1450}$ ), the host contamination is usually negligible, although may be significant for rare objects with excessive ongoing star formation. A more serious concern, however, is that some quasars may be heavily reddened by dust internal or external to the host. The so-called “dust-reddened” quasars (e.g., Glikman et al. 2007) have UV luminos-

ities significantly dust attenuated, and corrections are required to measure their intrinsic AGN luminosities. It is possible that optical quasar surveys (such as SDSS) are missing a significant population of dust-reddened quasars.

### 3.1.6 *Effects of orientation and radiation pressure*

If the BLR velocity distribution is not isotropic, orientation effects may affect the RM and SE mass estimates. Specific BLR geometry and kinematics, such as a flattened BLR where the orbits are confined to low latitudes, will lead to orientation-dependent line width. Some studies report a correlation between the broad line FWHM and the source orientation inferred from radio properties<sup>5</sup> (e.g., Wills & Browne 1986; Jarvis & McLure 2006), in favor of a flattened BLR geometry. Similar conclusions were achieved in Decarli et al. (2008a) based on somewhat different arguments. Since we use the average virial coefficient  $\langle f \rangle$  in our RM and SE mass estimates, the true BH masses in individual sources may be over- or underestimated depending on the actual inclination of the BLR (e.g., Krolik 2001; Decarli et al. 2008a; Fine et al. 2011; Runnoe et al. 2013)<sup>6</sup>. The distributions of broad line widths in bright quasars are typically log-normal, with dispersions of  $\sim 0.1 - 0.2$  dex over  $\sim 5$  magnitudes in luminosity (e.g., Shen et al. 2008a; Fine et al. 2008, 2010). A thin disk-like BLR geometry with a large range of inclination angles cannot account for such narrow distributions of line width, indicating either the inclination angle is limited to a narrow range for Type 1 objects, and/or there is a significant random velocity component (such as turbulent motion) of the BLR. This limits the scatter in BH mass estimates caused by orientation effects to be  $< 0.2 - 0.4$  dex.

So far we have assumed that the dynamics of the BLR is dominated by the gravity of the central BH. The possible effects of radiation pressure, which also has a  $\propto R^{-2}$  dilution as gravity, on the BLR dynamics have been emphasized by, e.g., Krolik (2001). On average the possible radiation effects are eliminated in the empirical calibration of the  $\langle f \rangle$  value (see §3.1.2), but neglecting such effects may introduce scatter in individual sources and luminosity-dependent trends. Most recently Marconi et al. (2008) modified the virial mass estimation by adding a luminosity term:

$$M_{\text{BH,M08}} = f \frac{W^2 R}{G} + g \left( \frac{L_{5100}}{10^{44} \text{ erg s}^{-1}} \right) M_{\odot}, \quad (6)$$

where the last term describes the effect of radiation pressure on the BLR dynamics with a free

---

<sup>5</sup>Some recent studies (e.g., Fine et al. 2011; Runnoe et al. 2013) argue that the dependence of line FWHM on source orientation is different for low-ionization and high-ionization lines, such that the CIV-emitting gas velocity field may be more isotropic than H $\beta$  and Mg II.

<sup>6</sup>Of some relevance here is the interpretation of the apparently small BH masses in a sub-class of Type 1 AGNs called narrow-line Seyfert 1s (NLS1s), where the H $\beta$  FWHM is narrower than  $2000 \text{ km s}^{-1}$  along with other unusual properties (such as strong iron emission and weak [O III] emission). Some argue (e.g., Decarli et al. 2008b) that NLS1s are preferentially seen close to face-on, hence their virial BH masses based on FWHM are underestimations of true masses. However, NLS1s also differ from normal Type 1 objects in ways that are difficult to explain with orientation effects (such as weak [O III] and strong X-ray variability). Orientation may play some role in the interpretation of NLS1s (especially for a minority of radio-loud NLS1s), but is unlikely to be a major factor.

parameter  $g$ . By allowing this extra term, Marconi et al. (2008) re-calibrated the RM masses using the  $M_{\text{BH}} - \sigma_*$  relation, and the SE mass estimator using the new RM masses. This approach improves the rms scatter between single-epoch masses and RM masses, from  $\sim 0.4$  dex to  $\sim 0.2$  dex, and removes the slight systematic trend of the SE mass scatter with RM masses seen in Vestergaard & Peterson (2006). However, it is also possible that the reduction of scatter between the SE and RM masses is caused by the addition of fitting freedoms. Since the intrinsic errors on the RM masses are unlikely to be  $< 0.3$  dex, optimizing the SE masses relative to RM masses to smaller scatter may lead to blown-up errors when apply the optimized scaling relation to other objects. It would be interesting to split the RM sample in Marconi et al. (2008) in half and use one half for calibration and the other half for prediction, and see if similar scatter can be achieved in both subsets. The relevance of radiation pressure is also questioned by Netzer (2009), who used large samples of Type 1 and Type 2 AGNs from the SDSS to show that the radiation-pressure corrected virial masses lead to inconsistent Eddington ratio distributions in Type 1s and Type 2s, even though the [O III] luminosity distribution is consistent in the two samples. However, Marconi et al. (2009) argues that the difference in the “observed” Eddington ratio distributions does not mean that radiation pressure is not important, rather it could result from a broad range of column densities which are not properly described by single values of parameters in the radiation-pressure-corrected mass formula. These studies then revealed that using the simple corrected formula as provided in Marconi et al. (2008) does not provide a satisfactory recipe to account for radiation pressure in RM or SE mass estimates, and the relevance of radiation pressure and a practical method to correct for its effect are therefore still under active investigations (e.g., Netzer & Marziani 2010).

### 3.1.7 Comparison among different line estimators

There are both low-ionization and high-ionization broad lines in the restframe UV to near-infrared of the quasar spectrum. Despite different ionization potential and probably different BLR structure, several of them have been adopted as SE virial mass estimators. The most frequently used line-luminosity pairs include strong Balmer lines ( $H\alpha$  and  $H\beta$ ) with  $L_{5100}$  or  $L_{H\alpha, H\beta}$ , Mg II with  $L_{3000}$ , and CIV with  $L_{1350}$  or  $L_{1450}$ . Hydrogen Paschen lines in the near-IR can also be used if such near-IR spectroscopy exists.

There have been SE calibrations upon specific lines against RM masses, or against SE masses based on another line. Comparisons between different SE line estimators using various quasar samples are often made in the literature: some claim consistency, while others report discrepancy. As emphasized in Shen et al. (2008a), it is important to use a consistent method in measuring luminosity and line width with that used for the calibrations if one wants to make a fair comparison using external samples. Failure to do so may lead to unreliable conclusions (e.g., Dietrich & Hamann 2004).

The continuum luminosities at different wavelengths and several line luminosities are all correlated with each other, with different levels of scatter. Fig. 2 shows some correlations between different continuum luminosities using the spectral measurements of SDSS quasars from Shen et al.



(2011). To compare  $L_{1350}$  and  $L_{5100}$  directly, one needs either UV+optical or optical+near-IR to cover both restframe wavelengths. Fig. 3 (left) shows such a comparison from a recent sample of quasars with optical spectra from SDSS and near-IR spectra from Shen & Liu (2012), which probes a higher luminosity range  $L_{5100} > 10^{45.4} \text{ erg s}^{-1}$  than the SDSS sample. Correlations between these luminosities are still seen at the high-luminosity end. For the SDSS quasar population, different luminosities correlate with each other well, but this may be somewhat affected by the optical target selection of SDSS quasars that may preferentially miss dust-reddened quasars (see §3.1.5). In other words, the intrinsic dispersion in the UV-optical SED may be larger for the general quasar population. For instance, Assef et al. (2011) found a much larger dispersion in the  $L_{1350}/L_{5100}$  ratio for a gravitationally lensed quasar sample, which is selected differently from the SDSS. This large dispersion in the  $L_{1350}/L_{5100}$  ratio will lead to more scatter between the  $H\beta$  and C IV based SE masses.

It is also important to compare the widths of different lines. Since  $H\beta$  is the most studied line in reverberation mapping and the  $R - L$  relation was measured using BLR radius for  $H\beta$  (e.g., Kaspi et al. 2000, 2005; Bentz et al. 2009a), it is reasonable to argue that the SE mass estimators based on the Balmer lines are the most reliable ones. The width of the broad  $H\alpha$  is well correlated with that of the broad  $H\beta$  and therefore it provides a good substitution in the absence of  $H\beta$  (e.g., Greene & Ho 2005). The widths of Mg II are found to correlate well with those of the Balmer lines (e.g., Salviander et al. 2007; McGill et al. 2008; Shen et al. 2008a, 2011; Wang et al. 2009; Vestergaard et al. 2011; Shen & Liu 2012, see Fig. 2 for a comparison based on SDSS quasars). But such a correlation may not be linear: despite different methods to measure line widths, most recent studies favor a slope shallower than unity in the correlation between the two FWHMs (e.g., see Fig. 2). Given this correlation it is practical to use the Mg II width as a surrogate for  $H\beta$  width in a Mg II-based SE mass estimators, and some recent Mg II calibrations can be found in, e.g., Vestergaard & Osmer (2009); Shen & Liu (2012); Trakhtenbrot & Netzer (2012). However, one intriguing feature regarding the Mg II line is that the distribution of its line widths seem to have small dispersions in large quasar samples (e.g., Shen et al. 2008a; Fine et al. 2008). It appears as if the Mg II varies at a less extent compared with  $H\beta$  (cf., Woo 2008, and references therein). It is also recently argued that for a small fraction of quasars ( $\sim 10\%$ ) in the NLS1 regime (e.g., small  $H\beta$  FWHM and strong Fe II emission), Mg II may have a blueshifted, non-virial component, and an overall larger FWHM than  $H\beta$ , that will bias the virial mass estimate (e.g., Marziani et al. 2013). This is consistent with the general trend found between Mg II and  $H\beta$  FWHMs using SDSS quasars (e.g., Wang et al. 2009; Shen et al. 2011; Vestergaard et al. 2011), and may be connected to the disk wind scenario for C IV discussed below.

The correlation between  $H\beta$  (or Mg II) and C IV widths is more controversial. While some claim that these two do not correlate well (e.g., Bachev et al. 2004; Baskin & Laor 2005; Netzer et al. 2007; Shen et al. 2008a; Fine et al. 2010; Shen & Liu 2012; Trakhtenbrot & Netzer 2012), others claim there is a significant correlation (e.g., Vestergaard & Peterson 2006; Assef et al. 2011). Fig. 3 (right) shows a compilation of C IV and  $H\beta$  FWHMs from the literature, which are derived for quasars in different luminosities and redshift ranges. Only the low-luminosity (and low- $z$ ) RM sample in Vestergaard & Peterson (2006) shows a significant correlation. It is often argued that sufficient data quality is needed to secure the C IV FWHM measurements, although measurement

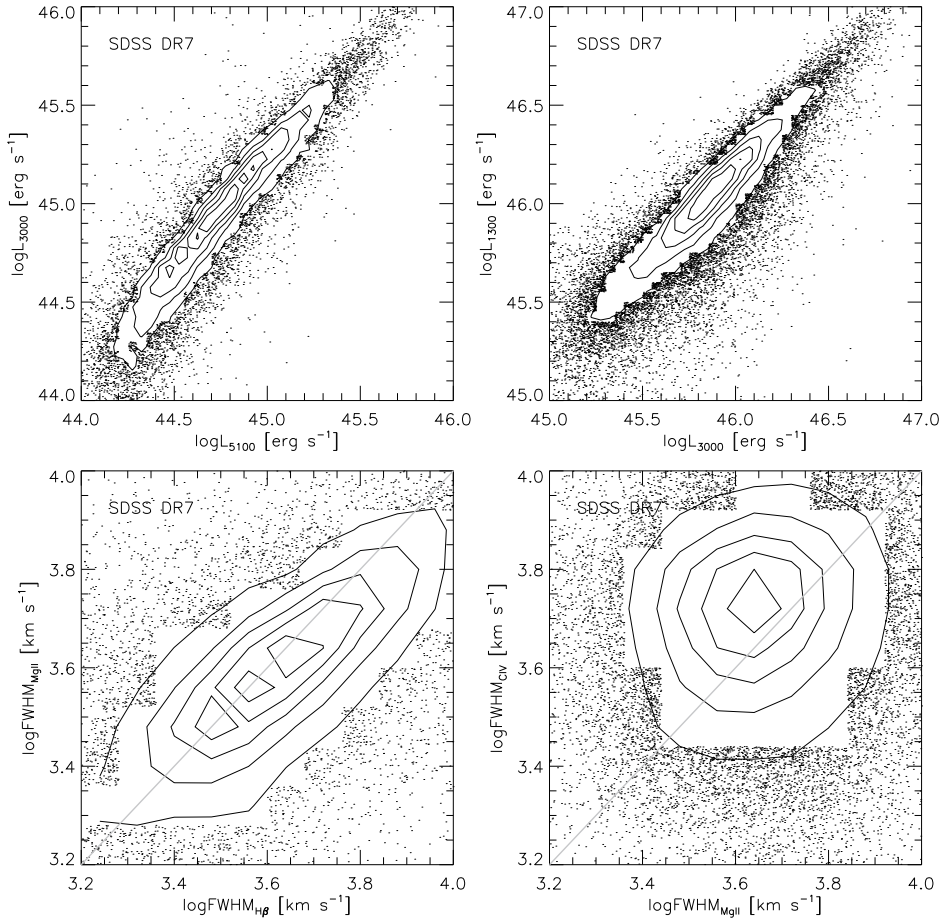


**Figure 2.** Comparisons between different continuum luminosities and line FWHMs, using SDSS quasar spectra that cover two lines. Shown here are the local point density contours. Measurements are from Shen et al. (2011). The upper panels show the correlations between continuum luminosities, and the bottom panels show the correlations between line FWHMs. While the Mg II FWHM correlates with H $\beta$  FWHM reasonably well, the correlation between the CIV FWHM and Mg II FWHM is poor (also see, e.g., Shen et al. 2008a; Fine et al. 2008, 2010).

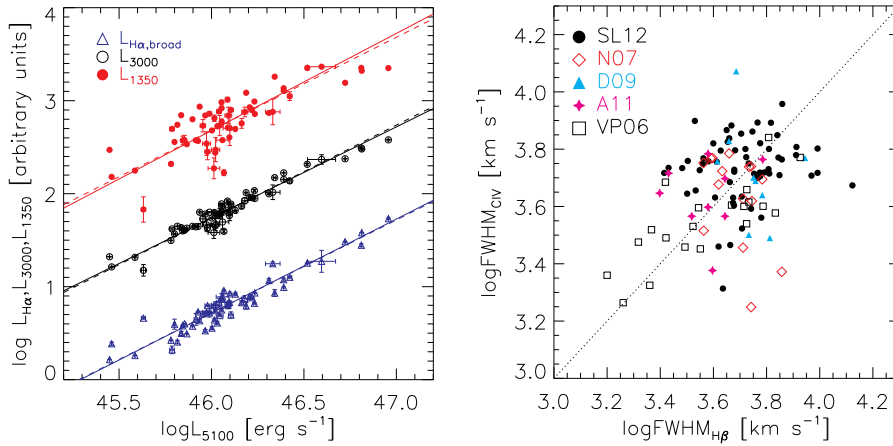


**Figure 3.** *Left:* correlations between different luminosities using the quasar sample in Shen & Liu (2012), which covers all four lines (CIV, Mg II, H $\beta$ , H $\alpha$ ) in the same object, for the high-luminosity regime  $L_{5100} > 10^{45.4}$  erg s<sup>-1</sup>. The solid lines are the bisector linear regression results using the BCES estimator (e.g., Akritas & Bershady 1996), and the dashed lines indicate a linear correlation of unity slope. *Right:* comparison between CIV FWHM and H $\beta$  FWHM using different samples from the literature [Shen & Liu (2012, 60 objects; SL12), Assef et al. (2011, 9 objects; A11), Vestergaard & Peterson (2006, 21 objects; VP06), Netzer et al. (2007, 15 objects; N07), and Dietrich et al. (2009, 9 objects; D09)]. Only for the low-redshift and low-luminosity VP06 sample is there a significant correlation between the two FWHMs.

errors are unlikely to account for all the scatter seen in the comparison between CIV and H $\beta$  FWHMs – the correlation between the two is still considerably poorer than that between Mg II and H $\beta$  FWHMs for the samples in Fig. 3 when restricted to high-quality data. Shen & Liu (2012) suggested that the reported strong correlation between CIV and H $\beta$  FWHMs is probably caused by the small sample statistics, or only valid for low-luminosity objects.

The high-ionization CIV line also differs from low-ionization lines such as Mg II and the Balmer lines in many ways (for a review, see Sulentic et al. 2000b). Most notably it shows a prominent blueshift (typically hundreds, up to thousands of km s<sup>-1</sup>) with respect to the low-ionization lines (e.g., Gaskell 1982; Tytler & Fan 1992; Richards et al. 2002), which becomes more prominent when luminosity increases. There is also a systemic trend (albeit with large scatter) of increasing CIV FWHM and line asymmetry when the CIV blueshift increases, a trend not present for low-ionization lines (e.g., Shen et al. 2008a, 2011). The CIV blueshift is predominantly believed to be an indication of outflows in some form, and integrated in the disk-wind framework discussed below (but see Gaskell 2009, for a different interpretation). These properties of CIV motivated the idea that CIV is likely more affected by a non-virial component than low-ionization lines (e.g., Shen et al. 2008a), probably from a radiatively-driven (and/or MHD-driven) accretion disk wind (e.g., Konigl & Kartje 1994; Murray et al. 1995; Proga et al. 2000; Everett 2005), especially for high-luminosity objects. A generic two-component model for the CIV emission is then implied (e.g., Collin-Souffrin et al. 1988; Richards et al. 2011; Wang et al.

2011). A similar argument is proposed by Denney (2012) based on the C<sub>IV</sub> RM data of local AGNs, where she finds that there is a component of the C<sub>IV</sub> line profile that does not reverberate, which is likely associated with the disk wind (although alternative interpretations exist). This may also explain the poorer correlation between C<sub>IV</sub> width and H $\beta$  (or Mg II) width for more luminous quasars, where the wind component is stronger (see further discussion in §3.1.9). Therefore C<sub>IV</sub> is likely a biased virial mass estimator (e.g., Baskin & Laor 2005; Sulentic et al. 2007; Netzer et al. 2007; Shen et al. 2008a; Marziani & Sulentic 2012, and references therein).

Although in principle certain properties of C<sub>IV</sub> (such as line shape parameters) can be used to infer the C<sub>IV</sub> blueshift and then correct for the C<sub>IV</sub>-based SE mass, such corrections are difficult in practice given the large scatter in these trends and typical spectral quality. Proponents on the usage of C<sub>IV</sub> line often emphasize the need for good-quality spectra and proper measurements of the line width. But the fact is C<sub>IV</sub> is indeed more problematic than the other lines, and there is no immediate way to improve the C<sub>IV</sub> estimator for high-redshift quasars, although some recent works are showing some promising trends that may be used to improve the C<sub>IV</sub> estimator (e.g., Denney 2012).

There have also been proposals for using the C<sub>III]</sub>, Al<sub>III</sub>, or Si<sub>III]</sub> lines in replacement of C<sub>IV</sub> (e.g., Greene et al. 2010a; Marziani & Sulentic 2012). Shen & Liu (2012) found that the FWHMs of C<sub>IV</sub> and C<sub>III]</sub> are correlated with each other, and hence C<sub>III]</sub> may not be a good line either (also see Ho et al. 2012). On the other hand, Al<sub>III</sub> and Si<sub>III]</sub> are more difficult to measure given their relative weakness compared to C<sub>IV</sub> and C<sub>III]</sub> as well as their blend nature, hence are not practical for large samples of quasars. Another possible line to use is Ly $\alpha$ . Although Ly $\alpha$  is more severely affected by absorption, intrinsically it may behave similarly as the Balmer lines. Such an investigation is ongoing.

To summarize, currently the most reliable lines to use are the Balmer lines, although this conclusion is largely based on the fact that these are the most studied and best understood lines, and does not mean there is no problem with them. Mg II can be used in the absence of the Balmer lines, although the lack of RM data for Mg II poses some uneasiness in its usage as a SE estimator. C<sub>IV</sub> has local RM data (though not enough to derive a  $R - L$  relation on its own), but the application of C<sub>IV</sub> to high-redshift and/or high-luminosity quasars should proceed with caution. In light of the potential problems with C<sub>IV</sub>, efforts have been underway to acquire near-IR spectroscopy to study the high- $z$  quasar BH masses using Mg II and Balmer lines (e.g., Shemmer et al. 2004; Netzer et al. 2007; Marziani et al. 2009; Dietrich et al. 2009; Greene et al. 2010a; Trakhtenbrot et al. 2011; Assef et al. 2011; Shen & Liu 2012; Ho et al. 2012; Matsuoka et al. 2013).

### 3.1.8 *Effects of AGN variability on SE masses*

Quasars and AGNs vary on a wide range of timescales. It is variability that made reverberation mapping possible in the first place. One might be concerned that the SE masses may subject to changes due to quasar variability. Several studies have shown, using multi-epoch spectra of

quasars, that the scatter due to luminosity changes (and possibly corresponding changes in line width) does not introduce significant ( $\gtrsim 0.1$  dex) scatter to the SE masses (e.g., Wilhite et al. 2007; Denney et al. 2009b; Park et al. 2012a). This is expected, since the average luminosity variability amplitude of quasars is only  $\sim 0.1 - 0.2$  magnitude over month-to-year timescales (e.g., Sesar et al. 2007; MacLeod et al. 2010; MacLeod et al. 2012), thus the difference in SE masses from multi-epochs will be dominated by measurement errors (in particular those on line widths).

However it is legitimate to consider the consequence of uncorrelated stochastic variations between line width and luminosity on SE masses, whether or not such uncorrelated variations are due to actual physical effects, or due to improper measurements of the continuum luminosity and line widths. Examples are already given in §3.1.1, and more detailed discussion will be provided in §3.3.

### 3.1.9 Limitations of the RM AGN sample

Last but not least, the current RM sample is by no means representative of the general quasar/AGN population. It is a highly heterogeneous sample that poorly samples the high-luminosity regime of quasars, and most objects are at  $z < 0.3$ . This alone calls into question the reliability of extrapolations of locally-calibrated SE relations against these RM AGNs to high- $z$  and/or high-luminosity quasars.

The distribution of the RM AGNs in the spectral parameter space of quasars is also highly biased relative to the general population. Richards et al. (2011) developed (building on earlier ideas by, e.g., Collin-Souffrin et al. 1988; Murray et al. 1995; Proga et al. 2000; Elvis 2000; Leighly & Moore 2004; Leighly 2004) a generic picture of two-component BLR structure for C IV, composed of a virial component, and a non-virial wind component which is filtering the ionizing continuum from the inner accretion disk. This generic picture is able to explain, phenomenologically, many characteristics of the continuum and C IV line properties, such as the C IV blueshift and the Baldwin effect (i.e., the anti-correlation between C IV equivalent width and adjacent continuum luminosity, Baldwin 1977). Fig. 4 shows the distribution of RM objects in the parameter space of C IV spectral properties, where most RM AGNs occupy the regime dominated by the virial component. Part of this is driven by luminosity, since more luminous quasars have on average larger C IV blueshift (§3.1.7). It will be important to explore this under-represented regime with C IV RM at high-redshift, which has just begun (e.g., Kaspi et al. 2007). Although this is an immediate concern for C IV, Richards et al. (2011) made a fair argument that the BLR properties for H $\beta$  and Mg II may also be biased in the RM sample relative to all quasars, if the non-virial wind component is also affecting the BLR of H $\beta$  and Mg II by filtering the ionizing continuum.

To date most of the RM lag measurements are for H $\beta$ , and lag measurements are either lacking for Mg II (but see Metzroth et al. 2006; Woo 2008, and references therein, for Mg II RM attempts and tentative results) or insufficient for C IV to derive a direct  $R - L$  relation based on these two UV lines. The total number of RM AGNs is also small,  $\sim 50$ , not enough to probe

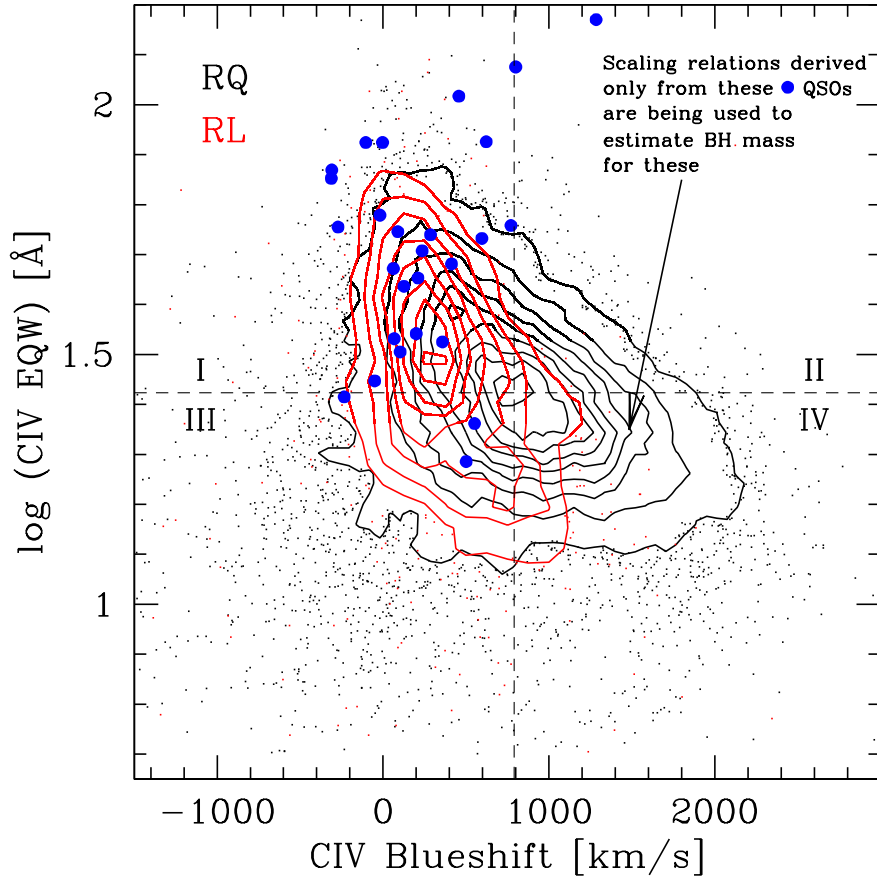


**Figure 4.** An updated version of Fig. 18 in Richards et al. (2011), showing the biased distribution of the local RM AGNs in the parameter space for CIV (blueshift relative to Mg II versus the rest equivalent width). The contours and dots are  $1.5 \lesssim z \lesssim 2.2$  SDSS quasars, and the blue filled circles are RM AGNs. The black and red contours show the results for radio-quiet and radio-loud populations respectively. Most of the RM AGNs occupy quadrant I, where the CIV line is dominated by the virial component in the two-component picture in Richards et al. (2011). In this picture, quadrant IV is for CIV lines dominated by the non-virial wind component. The average quasar luminosity increases from quadrant I to quadrant IV. Figure courtesy of G. Richards.

the diversity in BLR structure and other general quasar properties. The current sample size and inhomogeneity of RM AGNs pose another major obstacle to develop precise BH mass estimators based on RM and its extension, SE virial methods.

### 3.2 Practical Concerns

#### 3.2.1 *How to measure the continuum luminosity and line widths*

Usually the continuum and line properties are measured either directly from the spectrum, or derived from  $\chi^2$  fits to the spectrum with some functional forms for the continuum and for the lines. Arguably functional fits are better suited for spectroscopic samples with moderate to low spectral quality. As briefly mentioned earlier (§3.1.7), it is essential to measure the continuum and line width properly when using the existing SE calibrations. Different methods sometimes do yield systematically different results, in particular for the line width measurements. Some studies fit the broad lines with a single component (e.g., McLure & Dunlop 2004), while others use multiple components to fit the broad line. But if one wants to use the calibration in, e.g., McLure & Dunlop (2004), then it is better to be consistent with their fitting method. Some comparisons between the broad line widths from different fitting recipes can be made using the catalog provided in Shen et al. (2011). Take  $H\beta$  for example, since this broad line is not always a single Gaussian or Lorentzian, the line widths from the single-component and multiple-component fit could differ significantly in some cases.

The detailed description of spectral fitting procedure can be found in many papers (e.g., McLure & Dunlop 2004; Greene & Ho 2005; Shen et al. 2008a, 2011; Shen & Liu 2012). In short, the spectrum is first fit with a power-law plus an iron emission template<sup>7</sup> in several spectral windows free of major broad lines. The best-fit “pseudo-continuum” is then subtracted from the original spectrum, leaving the emission line spectrum. The broad line region is then fit with a mixture of functions (such as multiple Gaussians or Gauss-Hermite polynomials). The continuum luminosity and line width are then extracted from the best-fit model. The measurement errors from the multiple component fits are often estimated using some Monte Carlo methods (e.g., Shen et al. 2011; Shen & Liu 2012): mock spectra are generated either by adding noise to the original spectrum, or by adding “scrambled” residuals from the data minus best-fit model back to the model. The mock spectra are then fit with the same fitting procedure, and the formal errors are estimated from the distributions of the measured quantity from the mocks. This mock-based error estimation approach takes into account both the noise of the spectrum and ambiguities in decomposing different components in the fits.

---

<sup>7</sup>Empirical iron emission templates in the rest-frame UV to optical can be found in, e.g., Boroson & Green (1992); Vestergaard & Wilkes (2001); Tsuzuki et al. (2006). Using different iron templates may lead to small systematic offsets ( $\lesssim 0.05$  dex) in the measured continuum luminosity and line width (e.g., Nobuta et al. 2012). Occasionally a Balmer continuum component is added in the pseudo-continuum fit to improve the fit around the “small blue bump” region near 3000Å (e.g., Grandi 1982; Dietrich et al. 2002), but such a component is generally difficult to constrain from spectra with limited wavelength coverage (see discussions in, e.g., Wang et al. 2009; Shen & Liu 2012).

Below are some additional notes regarding continuum and line measurements.

- *Narrow line subtraction* Since the narrow line region (NLR) dynamics is not dominated by the central BH gravity, we want to subtract strong narrow line component before we measure the broad line width from the spectrum. This is particularly important for FWHM measurements, while for  $\sigma_{\text{line}}$  the effects of narrow lines are less important. For  $H\beta$  and  $H\alpha$ , reliable constraints on the velocity and width of the narrow components can be obtained from the adjacent narrow lines such as  $[O\text{ III}]\lambda\lambda 4959, 5007$  and  $[S\text{ II}]\lambda\lambda 6717, 6731$ . For  $Mg\text{ II}$  and  $C\text{ IV}$ , this is not so simple mainly for two reasons: 1) there are usually no adjacent strong narrow lines such as  $[O\text{ III}]$  to provide constraints on the narrow line component; and even if  $[O\text{ III}]$  can be covered in other wavelengths there is no guarantee the NLR properties are the same for  $[O\text{ III}]$  and for  $Mg\text{ II}/C\text{ IV}$ . 2) Although some quasars do show evidence of narrow component  $Mg\text{ II}$  and  $C\text{ IV}$ , it is unclear if this applies to the general quasar population. Shen & Liu (2012) found that for the 60 high-luminosity ( $L_{5100} > 10^{45.4}$  erg s $^{-1}$ ) quasars in their sample with optical and near-IR spectroscopy covering  $C\text{ IV}$  to  $[O\text{ III}]$ , the contribution of the narrow line component to  $C\text{ IV}$  is too small to affect the estimated broad  $C\text{ IV}$  FWHM significantly. However, for less luminous objects, the relative importance of the narrow line component to  $C\text{ IV}$  might be larger (e.g., Bachev et al. 2004; Sulentic et al. 2007).
- *Remedy for absorption* Sometimes there are absorption features superposed on the spectrum, which is most relevant for  $C\text{ IV}$ , and then  $Mg\text{ II}$ . Not accounting for these absorption features will bias the continuum and line measurements. While for narrow or moderately-broad absorption troughs, manual or automatic treatments can greatly minimize their effects (e.g., Shen et al. 2011), there is no easy way to fit objects that are heavily absorbed (such as broad absorption line quasars).
- *Effects of low signal-to-noise ratio (S/N)* The quality of the continuum luminosity and line width measurements decreases as the quality of the spectrum degrades. In addition to increased measurement errors, low S/N data may also lead to biases in the spectral measurements. Denney et al. (2009b) performed a detailed investigation on the effects of S/N on the measured  $H\beta$  line width using many single-epoch spectra of two RM AGNs (NGC 5548 and PG1229+204). They tested both direct measurements and Gauss-Hermite polynomial fits to the spectrum, and found that the best-fit line width is systematically underestimated at low S/N for both direct measurements and functional fits. The only exception is that their Gauss-Hermite fits to degraded NGC 5548 spectra tend to overestimate the FWHM at lower S/N. However, this is mainly caused by the fact that the Gauss-Hermite model is often unable to accurately fit the complex  $H\beta$  line profile of NGC 5548. Using multiple-Gaussian model fits, and for a much larger sample of SDSS quasars, Shen et al. (2011) also investigated the effects of S/N on the model fits by artificially degrading high S/N spectra (see their Figs. 5-8). They found that the exact magnitude of the bias depends on the line profile as well as the strength of the line. The continuum is usually unbiased as S/N decreases. The FWHMs and equivalent widths (EWs) are biased by less than  $\pm 20\%$  for high-EW objects as S/N is reduced to as low as  $\sim 3/\text{pixel}$ . For low-EW objects, the



FWHMs and EWs are biased low/high by  $> 20\%$  for  $S/N \lesssim 5/\text{pixel}$ . But the direction of the bias in FWHM is not always underestimation.

### 3.3 Consequences of the Uncertainties in SE Mass Estimates

Given the many physical and practical concerns discussed in §§3.1 and 3.2, one immediately realizes that these mass estimates, especially those SE mass estimates, should be interpreted with great caution. Almost everyone acknowledges the large uncertainties associated with these mass estimates, but only very few are taking these uncertainties seriously. Since at present there is no way to know whether or not the extrapolation of these SE methods to high- $z$  and/or high-luminosity quasars introduces significant biases, let us assume naively that these SE estimators provide unbiased mass estimates in the average sense, and focus on the statistical uncertainties (scatter) of these estimators.

In mathematical terms, we have:

$$m_e|m = m + G(0, \sigma_{SE}), \quad (7)$$

where  $m_e \equiv \log M_{\text{BH,SE}}$  is the SE mass estimate,  $m \equiv M_{\text{BH}}$  is the true BH mass, and  $G(\mu, \sigma)$  is a Gaussian random deviate with mean  $\mu$  and dispersion  $\sigma$ . I use  $x|y$  to denote a random value of  $x$  at fixed  $y$  drawn from the conditional probability distribution  $p(x|y)$ . Eqn. (7) thus means that the distribution of SE masses given true BH mass,  $p_0(m_e|m)$ , is a lognormal with mean equal to  $m$  and dispersion  $\sigma_{\text{SE}}$ . It is then clear that this equation stipulates our assumption that the SE mass is on average an unbiased estimate of the true mass, but with a statistical scatter of  $\sigma_{\text{SE}} \sim 0.5$  (dex), i.e., the formal uncertainty of SE masses.

#### 3.3.1 The Malmquist-type bias (Eddington bias)

Now let us assume that we have a mass-selected sample of objects with known true BH masses, and “observed” masses based on the SE estimators. By “mass-selected” I mean there is no selection bias caused by a flux (or luminosity) threshold – all BHs are observed regardless of their luminosity. If we further assume that the distribution of true BH masses in this sample is bottom-heavy, then a statistical bias in the SE masses naturally arises from the errors of SE masses (e.g., Shen et al. 2008a; Kelly et al. 2009a; Shen & Kelly 2010; Kelly et al. 2010), because there are more intrinsically lower-mass objects scattering into a SE mass bin due to errors than do intrinsically higher-mass objects. This statistical bias can be shown analytically assuming simple analytical forms of the distribution of true BH masses. Suppose the underlying true mass distribution is a power-law,  $dN/dM_{\text{BH}} \propto M_{\text{BH}}^{\gamma_M}$ , then Bayes’s theorem tells us the distribution of true BH masses at given SE mass is (recall  $p_0(m_e|m)$  is the conditional probability distribution of  $m_e$

given  $m$ ):

$$p_1(m|m_e) = p_0 10^{\gamma_M m} \left[ \int p_0 10^{\gamma_M m} dm \right]^{-1} = (2\pi\sigma_{SE}^2)^{-1/2} \exp \left\{ -\frac{[m - (m_e + \ln(10)\gamma_M\sigma_{SE}^2)]^2}{2\sigma_{SE}^2} \right\}. \quad (8)$$

Thus the expectation value of true mass at given SE mass is:

$$\langle m \rangle_{m_e} = m_e + \ln(10)\gamma_M\sigma_{SE}^2. \quad (9)$$

Therefore for bottom-heavy ( $\gamma_M < 0$ ) true mass distributions, the average true mass at given SE mass is smaller by  $-\ln(10)\gamma_M\sigma_{SE}^2$  dex than the SE mass. This has an important consequence that the quasar black hole mass function (BHMF) constructed using SE virial masses will be severely overestimated at the high-mass end (e.g., Kelly et al. 2009a, 2010; Shen & Kelly 2012).

This statistical bias due to the uncertainty in the mass estimates and a non-flat true mass distribution is formally known as the Eddington bias (Eddington 1913). Historically this has also been referred to as the Malmquist bias in studies involving distance estimates (e.g., Lynden-Bell et al. 1988), which bear some resemblance to the familiar Malmquist bias in magnitude-limited samples (e.g., Malmquist 1922). For this reason, this bias was called the ‘‘Malmquist’’ or ‘‘Malmquist-type’’ bias in Shen et al. (2008a) and Shen & Kelly (2010), and I adopted this name here as well. Perhaps a better name for this class of biases is the ‘‘Bayes correction’’, which then also applies to the generalization of statistical biases caused by threshold data and correlation scatter (or measurement errors). The luminosity-dependent bias discussed next, and the Lauer et al. bias (Lauer et al. 2007) discussed in §4.3, can also be described by this name.

### 3.3.2 Luminosity-dependent bias in SE virial BH masses

Now let us take one step further, and consider the conditional probability distribution of  $m_e$  at fixed true mass  $m$  and fixed luminosity  $l \equiv \log L$ ,  $p(m_e|m, l)$ . If the SE mass distribution at given true mass is independent on luminosity, then we have  $p(m_e|m, l) = p(m_e|m)$ . This means that the SE mass is always unbiased in the mean regardless of luminosity. However, one may consider such a situation where  $p(m_e|m, l) \neq p(m_e|m)$ , which means the distribution of SE masses will be modified once one limits on luminosity. This is an important issue, since essentially all statistical quasar samples are flux-limited samples (except for heterogeneous samples, such as the local RM AGN sample), and frequently the SE mass distribution in finite luminosity bins is measured and interpreted.

Below I will explore this possibility and its consequences in detail. To help the reader understand these issues, here is an outline of the discussion that follows: 1) I will first formulate the basic equations to understand the (mathematical) origin of the uncertainty in SE mass,  $\sigma_{SE}$ ; 2) I will then provide physical considerations to justify this formulation; 3) The conditional probability distribution of SE mass at fixed true mass and luminosity  $p(m_e|m, l)$  is then derived, and I

demonstrate the two most important consequences: the luminosity-dependent bias, and the narrower distribution of SE masses at fixed true mass and luminosity than the SE mass uncertainty  $\sigma_{SE}$ ; 4) I then discuss current observational constraints on the luminosity-dependent bias and demonstrate its effect using a simulated flux-limited quasar sample.

1) *Understanding the origin of the uncertainty  $\sigma_{SE}$  in SE masses*

I will use Gaussians (lognormal) to describe most distributions and neglect higher-order moments, mainly because the current precision and our understanding of SE masses are not sufficient for more sophisticated modeling. Assuming the distributions of luminosity and line width at given true mass  $m$  both follow lognormal distributions, we can write such distributions as

$$l|m = \langle l \rangle_m + G_1(0, \sigma_l), \quad w|m = \langle w \rangle_m + G_2(0, \sigma_w), \quad (10)$$

where notations are the same as in Eqn. (7),  $w \equiv \log W$ , and  $\langle \cdot \rangle_m$  indicates the expectation value at  $m$ . The dispersions in luminosity and line width at this fixed true mass should be understood *as due to both variations in single objects (i.e., variability) and object-by-object variance*. The SE mass estimated using  $l$  and  $w$  are then (e.g., Eqn. 4):

$$m_e|m = bl + cw + \text{constant}, \quad (11)$$

where the last term ‘‘constant’’ absorbs coefficient  $a$  and other constants from SE mass calibrations. Now let us consider the following two scenarios:

A. In the ideal case where the SE method gives a perfect mass estimate, we have

$$G_1(0, \sigma_l) = -\frac{c}{b}G_2(0, \sigma_w), \quad (12)$$

i.e., the deviations in luminosity and line width from their mean values at given true mass are perfectly correlated. The resulting  $m_e$  distribution thus peaks at  $m$  with zero width, i.e.,  $m_e|m = m = b\langle l \rangle_m + c\langle w \rangle_m + \text{constant}$ .

B. In the realistic case, certain amount of the deviations in  $l$  and  $w$  from their mean values are uncorrelated with each other (either intrinsic or due to measurement errors). Without loss of generality, we can rewrite Eqn. (10) as

$$l|m = \langle l \rangle_m + G_1(0, \sigma'_l) + G_0(0, \sigma_{\text{corr}}), \quad w|m = \langle w \rangle_m + G_2(0, \sigma'_w) - \frac{b}{c}G_0(0, \sigma_{\text{corr}}), \quad (13)$$

where the *total* dispersions in the distributions of  $l$  and  $w$  are

$$\sigma_l = \sqrt{\sigma'^2_l + \sigma_{\text{corr}}^2}, \quad \sigma_w = \sqrt{\sigma'^2_w + (\sigma_{\text{corr}}b/c)^2}. \quad (14)$$

Eqn. (13) stipulates that some portions of the dispersions in  $l$  and  $w$ , described by  $\sigma_{\text{corr}}$ , are correlated and do not contribute to the dispersion (scatter) of  $m_e$  at  $m$ . On the other hand,

the remaining dispersions in  $l$  ( $\sigma'_l$ ) and in  $w$  ( $\sigma'_w$ ) are stochastic terms, and they combine to cause the dispersion of  $m_e$  at  $m$ :

$$m_e|m = m + bG_1(0, \sigma'_l) + cG_2(0, \sigma'_w) = m + G(0, \sigma_{\text{SE}}), \quad (15)$$

where

$$\sigma_{\text{SE}} = \sqrt{(b\sigma'_l)^2 + (c\sigma'_w)^2} \quad (16)$$

is the formal uncertainty in SE mass, i.e., the scatter in  $m_e$  at given true mass  $m$ .

Eqn. (13) through (16) provide a general description of SE mass error budget from luminosity and line width, and form the basis of the following discussion. From now on I will only consider the realistic case B.

## 2) Physical considerations on the variances $\sigma'_l$ , $\sigma'_w$ and $\sigma_{\text{corr}}$

Most of the studies to date have implicitly assumed  $\sigma'_l = 0$  in Eqn. (13), with the few exceptions in e.g., Shen et al. (2008a), Shen & Kelly (2010) and Shen & Kelly (2012).  $\sigma'_l = 0$  imposes a strong requirement that *all* the variations in luminosity are compensated by line width such that the uncertainty in SE masses now completely comes from the  $\sigma'_w$  part in line width dispersion. While this is what we hope for the SE method, there are physical and practical reasons to expect a non-zero  $\sigma'_l$ , as discussed in, e.g., Shen & Kelly (2012). Specifically we have the following considerations:

**(a)** the stochastic continuum luminosity variation and response of the BLR (hence the response in line width) are not synchronized, as resulting from the time lag in the reverberation of the BLR. The rms continuum variability on timescales of the BLR light-cross time is  $\sim 0.05$  dex using the ensemble structure function in, e.g., MacLeod et al. (2010);

**(b)** even with the same true mass, individual quasars have different BLR properties, and presumably the measured optical-UV continuum luminosity is not as tightly connected to the BLR as the ionizing luminosity. Both will lead to stochastic deviations of luminosity and line width from the perfect correlation (source-by-source variation in the virial coefficient  $f$ , scatter in the  $R - L$  relation, etc.). The level of this luminosity stochasticity is unknown but is at least  $0.2 - 0.3$  dex given the scatter in the  $R - L$  relation alone, and thus it is a major contributor to  $\sigma'_l$ ;

**(c)** although not explicitly specified in Eqn. (13), there are uncorrelated measurement errors in luminosity and line width; typical measurement error in luminosity for SDSS spectra (with  $S/N \sim 5 - 10/\text{pixel}$ , e.g., see fig. 4 of Shen et al. 2011) is  $\sim 0.02$  dex (statistical only), but increases rapidly at low  $S/N$ ;

**(d)** and finally, what we measure as line width does not perfectly trace the virial velocity. This is a concern for essentially all three lines, and for both of the two common definitions of line width (FWHM and  $\sigma_{\text{line}}$ ). Two particular concerns arise. First, single-epoch spectra do not provide a line width that describes the reverberating part of the line only, thus some portion of the line width

may not respond to luminosity variations. Second, if a line is affected by a non-virial component (say, CIV for instance), and if this component strengthens and widens when luminosity increases, the total line width would not respond to the luminosity variation as expected. As in (b), this contribution to the uncompensated (by line width) luminosity variance  $\sigma'_l$  is unknown, but could be as significant as in (b).

One extreme of (d) would be that line width has nothing to do with the virial velocity except for providing a mean value in the calibrations of Eqn. (4), as suggested by Croom (2011), i.e.,  $\sigma_{\text{corr}} = 0$ . In this case while the average SE masses are unbiased by calibration, the luminosity-dependent SE mass bias at given true mass is maximum (see below). Note that this  $\sigma_{\text{corr}} = 0$  case was already considered in Shen et al. (2008a) and Shen & Kelly (2010) when demonstrating the luminosity-dependent bias, and is only a special case of the above generalized formalism.

On the other hand,  $\sigma_{\text{corr}} > 0$  would mean that line width does respond to luminosity variations to some extent, justifying the inclusion of line width in Eqn. (4). This was indeed seen at least for some local, low-luminosity objects, although not so much for the high-luminosity SDSS sample, based on the tests described in §3.1.1; additional evidence is provided in, e.g., Kelly & Bechtold (2007) and Assef et al. (2012), again for the low-luminosity RM AGN sample. Therefore, the most realistic scenario is that at fixed true mass, some portions of the dispersions in luminosity (or equivalently, Eddington ratio) and in line width are correlated with each other, and they cancel out in the calculation of SE masses; the remaining portions of the dispersions in  $l$  and  $w$  are stochastic in nature and they combine to contribute to the SE mass uncertainty (as in Eqn. 16). In other words, we expect  $\sigma'_l > 0$ ,  $\sigma'_w > 0$ , and  $\sigma_{\text{corr}} > 0$ . For simplicity I take constant values for these scatters in the following discussion, but it is possible that they depend on true BH mass.

### 3) The distribution of SE mass at fixed true mass and luminosity $p(m_e|m, l)$

Now that we have formulated the distributions of  $l$ ,  $w$  and  $m_e$  at fixed  $m$  (e.g., Eqns. 11 and 13), we can derive the conditional probability distribution of  $m_e$  at fixed  $m$  and  $l$ ,  $p(m_e|m, l)$ . It is straightforward to show<sup>8</sup> (again using Bayes's theorem) that this distribution is also a Gaussian distribution, with mean and dispersion:

$$\langle m_e \rangle_{m,l} = m + \frac{b\sigma_l'^2}{\sigma_l'^2 + \sigma_{\text{corr}}^2} (l - \langle l \rangle_m), \quad \sigma_{ml}^2 = \frac{(b\sigma_l')^2 \sigma_{\text{corr}}^2}{\sigma_l'^2 + \sigma_{\text{corr}}^2} + (c\sigma_w')^2. \quad (17)$$

<sup>8</sup>Here I give one possible derivation. For brevity I will drop  $m$  in all probability distributions, but it should be understood that all these distributions are at fixed  $m$ . Consider the  $\sigma_w' = 0$  case first, where we want to derive  $p(m_e|l)$ . Using Bayes's theorem,  $p(m_e|l) \propto p(m_e)p(l|m_e)$ . We have  $p(m_e) \propto e^{-(m_e-m)^2/[2(b\sigma_l')^2]}$  (i.e., all variance in  $m_e$  comes from  $\sigma_l'$  since  $\sigma_w' = 0$ ), and  $p(l|m_e) \propto e^{-[l - (\frac{m_e-m}{b} + \langle l \rangle_m)]^2/(2\sigma_{\text{corr}}^2)}$  (i.e.,  $l$  can only vary due to  $\sigma_{\text{corr}}$  at fixed  $m_e$ ). Therefore  $p(m_e|l) \propto e^{-(m_e - \langle m_e \rangle_{m,l})^2/(2\sigma_{ml}^2)}$ , where  $\langle m_e \rangle_{m,l}$  is the same as in Eqn. (17), and  $\sigma_{ml}^2 = (b\sigma_l')^2 \sigma_{\text{corr}}^2 / (\sigma_l'^2 + \sigma_{\text{corr}}^2)$ . Now add back in the  $\sigma_w'$  term, which will convolve  $p(m_e|l)$  with a Gaussian distribution. Then the general distribution  $p(m_e|l)$  for arbitrary values of  $\sigma_w'$  is also a Gaussian, with the same mean, but a dispersion that is broadened by  $c\sigma_w'$  (i.e., the same as in Eqn. 17).

Therefore we can generate the distribution of  $m_e$  at fixed  $m$  and  $l$  as:

$$m_e|m, l = m + \beta(l - \langle l \rangle_m) + G(0, \sigma_{ml}), \quad (18)$$

where (using Eqns. 14 and 16)

$$\beta = \frac{b\sigma_l'^2}{\sigma_l'^2 + \sigma_{\text{corr}}^2} = \frac{b\sigma_l'^2}{\sigma_l^2}, \quad \sigma_{ml}^2 = \sigma_{\text{SE}}^2 - \beta^2\sigma_l^2 = (b\sigma_l')^2 + (c\sigma_w')^2 - \beta^2\sigma_l^2. \quad (19)$$

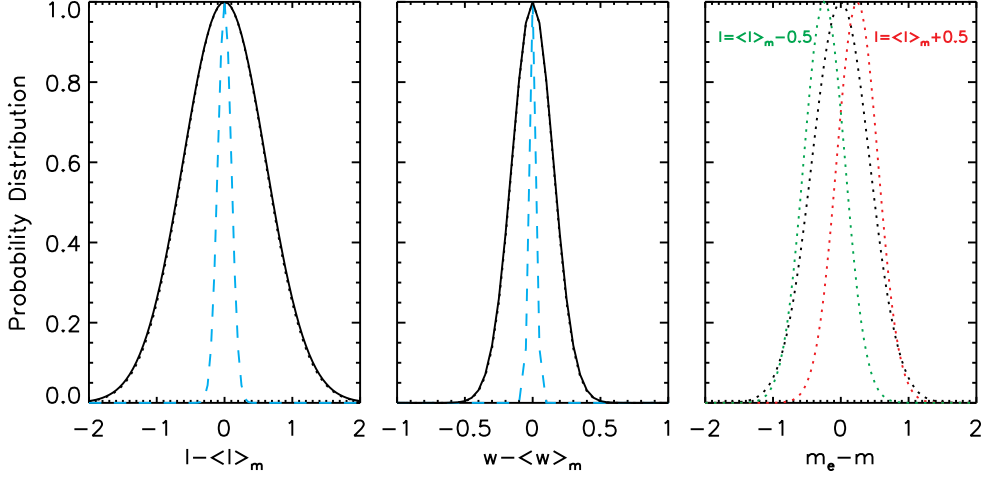
Physically  $\sigma_{ml}$  is the dispersion of SE mass at fixed true mass and fixed luminosity. The parameter  $\beta$  denotes the magnitude (slope) of the luminosity-dependent bias, and we have<sup>9</sup>  $0 < \beta < b$ , where the lower and upper boundaries correspond to the two extreme cases  $\sigma_l' = 0$  and  $\sigma_{\text{corr}} = 0$ . A larger  $\beta$  means a stronger luminosity-dependent bias. Given the values of  $\sigma_l'$ ,  $\sigma_w'$  and  $\sigma_{\text{corr}}$ , and a SE calibration ( $b$  and  $c$ ), all other quantities can be derived using Eqns. (14)-(19).

Fig. 5 shows a demonstration with  $\sigma_l' = 0.6$ ,  $\sigma_{\text{corr}} = 0.1$ ,  $\sigma_w' = 0.15$ ,  $b = 0.5$  and  $c = 2$ . In this example we have  $\beta = 0.49$ ,  $\sigma_{\text{SE}} = 0.42$ , and  $\sigma_{ml} = 0.3$ . The left two panels show the distributions of luminosity and line width at fixed true mass, from the stochastic term ( $\sigma_l'$ ,  $\sigma_w'$ ), the correlated term ( $\sigma_{\text{corr}}$ ) and the total dispersion ( $\sigma_l$ ,  $\sigma_w$ ). The right panel shows the distributions of SE masses at this fixed true mass for all luminosities (black dotted line) and for fixed luminosities (green and red dotted lines). The distributions of SE masses at fixed luminosity are both narrower and biased compared with the distribution without luminosity constraint.

There are two important conclusions that can be drawn from Eqns. (17)-(19):

- At fixed true mass  $m$ , the SE mass  $m_e$  is over-/underestimated when luminosity  $l$  is higher/lower than the average value at fixed  $m$ . This is the “luminosity-dependent bias” first introduced in Shen et al. (2008a) and subsequently developed in Shen & Kelly (2010) and Shen & Kelly (2012). The magnitude of this bias, determined by  $\beta$ , depends on how much of the dispersion in luminosity at fixed true mass is stochastic with respect to line width (i.e., not compensated by responses in  $w$ ).
- Secondly, the variance in SE masses at fixed true mass and fixed luminosity,  $\sigma_{ml}^2$ , is generally smaller than the uncertainty of SE masses,  $\sigma_{\text{SE}}^2$ , by an amount of  $(\beta\sigma_l)^2$ . A simple way to understand this is that the uncertainty (variance) of SE mass at fixed true mass comes from the stochastic variance terms in both luminosity and line width. Therefore when one reduces the variance in either luminosity or line width by fixing either variable, the variance in SE mass is also reduced. This has important consequences in interpreting the observed distribution of SE masses for quasars in flux-limited samples or in narrow luminosity bins. One *cannot* simply argue (as did in, e.g., Kollmeier et al. 2006; Steinhardt & Elvis 2010b) that the uncertainty in SE masses is small because the distribution of SE masses for samples

<sup>9</sup>For the sake of completeness, I note that  $\beta > b$  could happen, if the line width were actually positively correlated to luminosity in the  $\sigma_{\text{corr}}$  terms in Eqn. (13). Of course such a scenario is counter-intuitive (regarding the virial assumption) and thus unlikely, and it means one should not use line width at all in estimating SE masses.



**Figure 5.** Simulated distributions of  $l$  (left),  $w$  (middle), and  $m_e$  (right) at fixed true mass  $m$ , following the description in §3.3.2 (e.g., see Eqns. 13-19). The example shown here assumes  $b = 0.5$ ,  $c = 2$  in Eqn. (13), e.g., the typical values for SE mass estimators. *Left:* The distribution of luminosity  $l \equiv \log L$ . The black dotted line indicates the dispersion in  $\sigma'_l = 0.6$ , the cyan dashed line indicates the dispersion in  $\sigma_{\text{corr}} = 0.1$ , and the black solid line indicates the total dispersion in  $\sigma_l = \sqrt{\sigma_l'^2 + \sigma_{\text{corr}}^2}$  (which essentially overlaps with the dotted line given that  $\sigma_l$  is dominated by  $\sigma_l'$ ). *Middle:* The distribution of line width  $w \equiv \log W$ . The black dotted line indicates the dispersion in  $\sigma'_w = 0.15$ , the cyan dashed line indicates the dispersion in  $-\sigma_{\text{corr}}b/c$  (i.e., the part that correlates with luminosity), and the black solid line indicates the total dispersion in  $\sigma_w = \sqrt{\sigma_w'^2 + (\sigma_{\text{corr}}b/c)^2}$ . Again the solid line and the dotted line are almost on top of each other. *Right:* The distribution of SE mass  $m_e \equiv \log M_{\text{SE}}$ . The black dotted line indicates the total dispersion of  $m_e$  at fixed  $m$ ,  $\sigma_{\text{SE}} = \sqrt{(b\sigma_l')^2 + (c\sigma_w')^2} = 0.42$ . The green (red) dotted line indicates the distribution of  $m_e$  at fixed  $m$  and fixed  $l = \langle l \rangle_m - 0.5$  ( $\langle l \rangle_m + 0.5$ ), which is a Gaussian described by Eqns. (18)-(19). In this example most of the dispersions in luminosity and line width are uncorrelated with each other, leading to a large uncertainty in SE masses  $\sigma_{\text{SE}} = 0.42$  dex. The inferred luminosity-dependent bias has a slope of  $\beta = 0.49$ . The dispersion of  $m_e$  at fixed luminosity is only  $\sigma_{ml} = 0.3$  dex (Eqn. 19), much smaller than the uncertainty in SE masses,  $\sigma_{\text{SE}}$ .

with restricted luminosity ranges is narrow. The example shown in Fig. 5 clearly demonstrates that one can easily get a much narrower SE mass distribution at fixed true mass and luminosity, than the nominal SE mass uncertainty  $\sigma_{\text{SE}}$ . On the other hand, if enforcing  $\sigma'_l = 0$ , then  $\sigma_{\text{SE}} = c\sigma'_w < c\sigma_w$ , and there will be tension between the observed narrow distribution in line width (e.g., Shen et al. 2008a; Fine et al. 2008), which indicates  $\sigma_w \lesssim 0.15$  dex for Mg II, and the expectation that  $\sigma_{\text{SE}} > 0.3$  dex.

#### 4) Observational constraints on the luminosity-dependent bias

The exact value of  $\beta$  is difficult to determine observationally, although some rough estimates

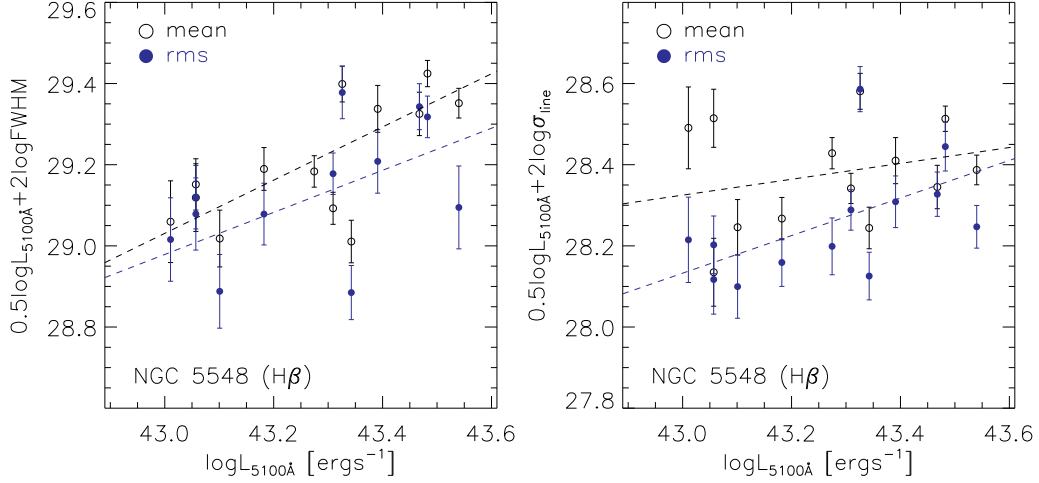


**Figure 6.** A test on a non-zero  $\beta$  using RM data for NGC 5548. Plotted here is the dependence of the virial products computed from 5100 $\text{\AA}$  continuum luminosity and line width as a function of luminosity, for NGC 5548 and for H $\beta$  only, for FWHM (left) and  $\sigma_{\text{line}}$  (right), respectively. This form of the virial product represents SE estimators with  $b = 0.5$  and  $c = 2$  in Eqn. (4), and I am using luminosity instead of time lag  $\tau$  in computing the virial product since I am testing SE mass estimators. The measurements were taken from Collin et al. (2006), which are based on both mean and rms spectra during each monitoring period. Error bars represent measurement errors. The error bars in luminosity have been omitted in the plot for clarity. The continuum luminosity has been corrected for host starlight using the correction provided by Bentz et al. (2009a). The black and blue dashed lines are the best linear-regression fits using the Bayesian method of Kelly (2007), for measurements based on mean and rms spectra, respectively. The residual correlation between the virial product and luminosity cannot be completely removed, and a positive  $\beta \sim 0.2 - 0.6$  is inferred in all cases, although the uncertainty in  $\beta$  is too large to rule out a zero  $\beta$  at  $> 3\sigma$  significance. Figure adapted from Shen & Kelly (2012).

can be made based on monitoring data of single objects, or samples of AGNs with known “true” mass (using RM masses or  $M_{\text{BH}} - \sigma_*$  masses). The former test constrains the stochasticity in single objects, while the latter test explores object-by-object variance. Using the intensively monitored H $\beta$  RM data for a single object, NGC 5548, Shen & Kelly (2012) tested the possibility of a non-zero  $\beta$ . The continuum luminosity of this object varied by  $\sim 0.5$  dex within a decade, providing a test on how good line width varies in accordance to luminosity variations for a single object and for a single line. Fig. 6 shows the change of SE masses as a function of the mean continuum luminosity in each monitoring year, computed using both FWHM and  $\sigma_{\text{line}}$  from both mean and rms spectra in each year. There is an average trend of increasing the SE masses as luminosity increases in all four cases, although the trend is less obvious for  $\sigma_{\text{line}}$ -based SE masses. The inferred value of  $\beta$ , using the linear regression method in Kelly (2007), is  $\sim 0.2-0.6$ , although the uncertainty in  $\beta$  is generally too large to rule out a zero  $\beta$  at  $> 3\sigma$  significance.



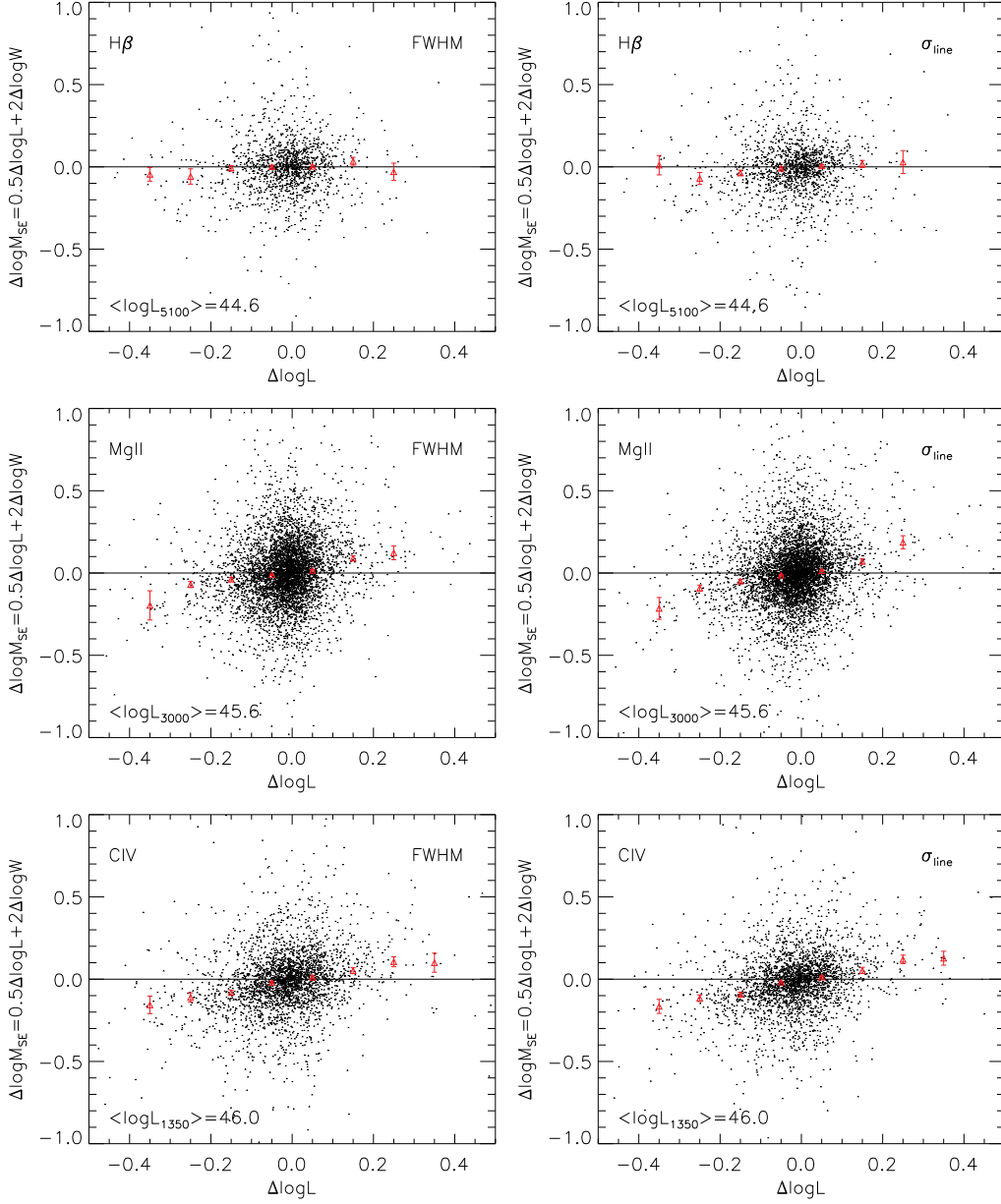


**Figure 7.** Tests of a non-zero  $\beta$  using two-epoch spectroscopy from SDSS (She, Shen, et al., in preparation). The data and notations are the same as in Fig. 1. The SE masses remain more or less constant as luminosity changes only for the low-luminosity and low- $z$  sample based on H $\beta$ . For the high-luminosity and high- $z$  samples based on Mg II and CIV, a luminosity-dependent bias in SE masses is inferred, with an error slope of  $\beta \sim 0.5$ .

A similar test is based on the repeated spectroscopy in SDSS (see discussion in §3.1.1). While most objects do not have a large dynamic range in luminosity variations in two epochs, the large number of objects allows a reasonable determination of the average trend of SE masses with luminosity, for the whole population of quasars. In addition, we want to include measurement uncertainties (both statistical and systematic), which allows us to make realistic constraints, as measurement errors will always be present. As shown in Fig. 1, the line width from single-epoch spectra does not seem to respond to luminosity variations except for low-luminosity objects based on  $H\beta$ , as expected from the physical/practical reasons I described above. I plot the changes in SE masses as a function of luminosity changes in Fig. 7. From this figure I estimate  $\beta \sim 0.5$  for the high- $L$  samples based on  $Mg\ II$  and  $CIV$ , and  $\beta \sim 0$  for the low- $L$  sample based on  $H\beta$  (She, Shen et al., in preparation). The difference in the low- $L$  (low- $z$ ) and high- $L$  (high- $z$ ) samples could be due to a luminosity effect, e.g., the correspondence between line width and luminosity variations is poorer at higher luminosities, or due to the difference between  $H\beta$  and the other two lines (She, Shen et al., in preparation).

Shen & Kelly (2012) also attempted to constrain  $\beta$  using forward Bayesian modeling of SDSS quasars in the mass-luminosity plane (see §4.2). While the results suggested a non-zero  $\beta \sim 0.2 - 0.4$ , the constraints were not very strong (see their fig. 11). Combining all these tests, we can conclude the following:  $\beta$  is probably smaller than  $\sim 0.5$  (i.e., line width still plays some physical role in SE mass estimates) but unlikely zero, although the exact value is uncertain. The value of  $\beta$  likely also depends on the specific line. More monitoring data of individual AGNs, and/or a substantially larger sample of AGNs with RM mass (or  $M_{BH} - \sigma_*$  masses) spreading enough dynamic range in luminosity at fixed mass, will be critical in better constraining  $\beta$ .

The effects of the luminosity-dependent bias on flux-limited samples are discussed intensively in, e.g., Shen et al. (2008a), Shen & Kelly (2010) and Shen & Kelly (2012). Here I use a simple simulation of a power-law true BH mass distribution,  $dN/dM_{BH} \propto M_{BH}^{-3.6}$ , to demonstrate these effects in Fig. 8. This steep true mass distribution was chosen to reproduce the distribution at the high-mass end for SDSS quasars (Shen et al. 2008a), which is certainly not appropriate at the low-mass end. I use the same example as in Fig. 5 for all the dispersion terms in luminosity and line width at fixed true mass. The true masses are distributed between  $5 \times 10^7 M_\odot$  and  $10^{10} M_\odot$  according to the specified power-law distribution. The mean luminosity at fixed  $m$  is determined assuming a constant Eddington ratio  $\lambda = 0.05$ . Then the instantaneous luminosity and SE mass at each true mass  $m$  are generated using Eqns. (13)-(19). The resulting distribution in the  $m - m_e$  plane is shown in black contours and points in Fig. 8, where I also show the distribution of a flux-limited (luminosity-limited) subset of BHs with  $l > \langle l \rangle_{m=8.3}$ , the mean luminosity corresponding to  $M_{BH} = 2 \times 10^8 M_\odot$ . The simulated distributions in luminosity, line width and SE virial masses are consistent with those for SDSS quasars when a similar flux limit is imposed on the simulated BHs. It is clear from Fig. 8 that for the flux-limited subset, the SE masses are biased high from the true masses. This is because in this simulation we have  $\beta = 0.49$ , which implies a significant luminosity-dependent bias at fixed true mass. Then the bottom-heavy BH mass distribution and the large scatter of luminosity at fixed true mass lead to more overestimated SE masses scattered upward than underestimated ones scattered downward, causing a net sample bias in SE masses (Shen et al. 2008a; Shen & Kelly 2010, 2012).

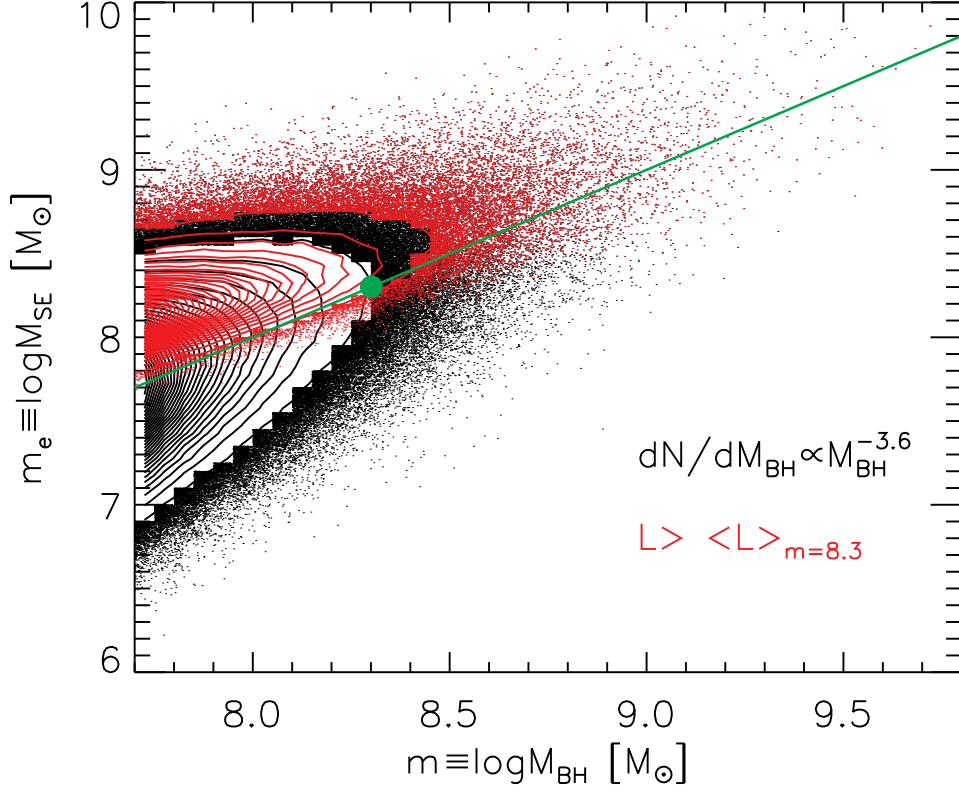


**Figure 8.** A simulated population of BHs with true masses  $M_{\text{BH}}$  within  $5 \times 10^7 - 10^{10} M_{\odot}$ , distributed as a power-law  $dN/dM_{\text{BH}} \propto M_{\text{BH}}^{-3.6}$ . I have assumed a constant Eddington ratio  $\lambda = 0.05$  to generate the mean luminosity  $\langle l \rangle_m$  at fixed true mass. I then used the dispersions specified by the example shown in Fig. 5 to generate instantaneous luminosity and SE masses. The resulting distributions in luminosity, line width and SE masses are consistent with those for the SDSS quasar sample (e.g., Shen et al. 2011). The black contours (local point density contours) and points show the distribution in the  $m_e - m$  plane. The green line shows the unity relation  $m_e = m$ . As expected, there is substantial scatter in  $m_e$  at fixed  $m$  due to the uncertainty in SE masses ( $\sigma_{\text{SE}} = 0.42$  dex). The red contours and points show the distribution for a subset of quasars with  $l > \langle l \rangle_{m=8.3}$ , the corresponding mean luminosity at  $M_{\text{BH}} = 2 \times 10^8 M_{\odot}$  (marked by the green circle). The SE masses are biased high from their true masses for this flux-limited sample (i.e., most points are above the unity relation) due to the substantial luminosity-dependent bias, the large dispersion in luminosity at fixed true mass, and the bottom-heavy true mass distribution in this example.

## 4. Applications to Statistical Quasar Samples

Despite the many caveats of SE mass estimators discussed above, they have been extensively used in recent years to measure BH masses in quasar and AGN samples over wide luminosity and redshift ranges, given their easiness to use. These applications include the Eddington ratio distributions of quasars, the demographics of quasars in terms of the black hole mass function (BHMF), the correlations between BH mass and host properties, and BH mass dependence of quasar properties. It is important to recognize, however, that these BH mass estimates are not true masses, and the uncertainty in these mass estimates has dramatic influences on the interpretation of these measurements.

Below I discuss several major applications of the SE virial mass estimators to statistical quasar samples. Other applications of these SE masses, such as quasar phenomenology, while equally important, will not be covered here.

### 4.1 Early Growth of SMBHs

One of the strong drivers for developing the SE virial mass technique is to estimate BH masses for high redshift quasars to better than a factor of ten accuracy, and to study the growth of SMBHs up to very high redshift (e.g., Vestergaard 2004). Such investigations have been greatly improved in the era of modern, large-scale spectroscopic surveys. The SDSS survey has been influential on this topic by providing more than tens of thousands of optical quasar spectra and SE mass estimates up to  $z \sim 5$  (e.g., McLure & Dunlop 2004; Netzer & Trakhtenbrot 2007; Shen et al. 2008a, 2011; Labita et al. 2009a,b). On the other hand, deeper and dedicated optical and near-IR spectroscopic programs are probing the SMBH growth to even higher redshift (e.g., Jiang et al. 2007; Kurk et al. 2007; Willott et al. 2010; Mortlock et al. 2011).

In Fig. 9 I show a compilation of SE virial mass estimates for quasars over a wide redshift range  $0 < z \lesssim 7$  from different studies. The black dots show the SE masses from the SDSS DR7 quasar sample (Schneider et al. 2010; Shen et al. 2011), which were estimated based on  $H\beta$  for  $z < 0.7$ ,  $Mg\ II$  for  $0.7 < z < 1.9$  and  $CIV$  for  $1.9 < z < 5$ . As discussed in §3.1.7, the reliability of  $CIV$ -based SE masses for the high- $z$  and high-luminosity quasars has been questioned, and several studies have obtained near-IR spectra for  $z \gtrsim 2$  quasars to get  $H\beta$ -based (filled symbols) and  $Mg\ II$ -based (open symbols) SE masses at high redshift. Albeit with considerable uncertainties and possible biases in individual SE mass estimates (all on the order of a factor of a few), these studies show that massive,  $\gtrsim 10^9 M_\odot$  BHs are probably already in place by  $z \sim 7$ , when the age of the Universe is only less than 1 Gyr. The abundance of these massive and active BHs then evolves strongly with redshift, showing the rise and fall of the bright quasar population with cosmic time.

One outstanding question regarding the observed earliest quasars is how they could have grown such massive SMBHs given the limited time they have, which is a non-trivial problem since the discoveries of  $z > 4$  quasars (e.g., Turner 1991; Haiman & Loeb 2001). One con-

cern is if these highest redshift quasars have their luminosities magnified by gravitational lensing or if their luminosities are strongly beamed (e.g., Wyithe & Loeb 2002; Haiman & Cen 2002), which will affect earlier estimates of their BH masses using the Eddington-limit argument. The lensing hypothesis will also lead to overestimated virial BH masses. However later deep, high-resolution imaging of  $z > 4$  quasars with HST did not find any multiple images around these objects (e.g., Richards et al. 2004b, 2006b), rendering the lensing hypothesis highly unlikely (e.g., Keeton et al. 2005). Strong beaming can also be ruled out based on the high values of the observed line/continuum ratio of these high-redshift quasars (e.g., Haiman & Cen 2002).

Given the  $e$ -folding time introduced in §1,  $t_e = 4.5 \times 10^8 \frac{\epsilon}{\lambda(1-\epsilon)}$  yr, and a seed BH mass  $M_{\text{seed}}$  at an earlier epoch  $z_i$ , the final mass at  $z_f \sim 6$  is

$$M_{\text{BH}} = M_{\text{seed}} \exp\left(\frac{t_f - t_i}{t_e}\right), \quad (20)$$

where  $t_f$  and  $t_i$  are the cosmic age at  $z_f$  and  $z_i$ , respectively.

Assuming continuous accretion with constant radiative efficiency  $\epsilon$  and luminosity Eddington ratio  $\lambda$  and *without mergers*, I showed in Fig. 9 three different growth histories from a seed BH at higher redshift. The solid lines are for a seed BH at  $z = 20$  and  $\lambda = 1$ , i.e., Eddington-limited accretion; the dashed lines are for a seed BH at  $z = 30$  and  $\lambda = 1$ ; the dotted lines are for a seed BH at  $z = 20$  and  $\lambda = 1.5$ , i.e., mildly super-Eddington accretion. For each model I used three seed BH mass,  $M_{\text{seed}} = 10, 20, 100 M_{\odot}$ , which encloses the reasonable ranges of predicted remnant BH mass from the first generation of stars (Pop III stars, for a review see, e.g., Bromm et al. 2009). Then it is clear from Fig. 9 that, if the accretion is Eddington-limited, it is difficult to grow  $\gtrsim 10^9 M_{\odot}$  BHs at  $z \sim 6$  from a Pop III remnant seed BH at  $z \sim 20 - 30$  (where such first stars were formed out of  $\sim 10^6 M_{\odot}$  halos, corresponding to  $\sim 3 - 4\sigma$  peaks in the density perturbation field). On the other hand, if allowing mildly super-Eddington accretion, then a  $\sim 10^9 M_{\odot}$  BH can be readily formed at  $z \sim 7$  from a large Pop III star remnant  $M_{\text{seed}} \sim 100 M_{\odot}$ , although more recent simulations suggest somewhat lower masses of Pop III stars due to possible effects of clump fragmentation and/or radiative feedback (e.g., Turk et al. 2009; Hosokawa et al. 2011; Stacy et al. 2012), and hence a lower typical value of the remnant mass of less than tens of solar masses. Mildly super-Eddington accretion (up to  $\lambda \sim$  a few) could happen, for instance, if the radiation and density fields of the accretion flow are anisotropic and most of the accretion flow is not impeded by the radiation force. Mergers between BHs at high- $z$  can also help with the required growth if the coalesced BH is not ejected from the halo by the gravitational recoil from the merger. The main challenge here is whether or not such critical accretion can maintain stable and uninterrupted for the entire time (e.g., Pelupessy et al. 2007). But in any case, it is quite likely that the observed  $z > 6$  quasars are all born in rare environments of the early Universe, thus extreme conditions (such as large gas density, high merger rate, etc.) may have facilitated their growth. Indeed, some theoretical studies can successfully produce such massive BHs at  $z \sim 6$  growing from a typical Pop III remnant BH seed without super-Eddington accretion (e.g., Yoo & Miralda-Escude 2004; Li et al. 2007; Tanaka & Haiman 2009). But the detailed physics (accretion rate, mergers, BH recoils, etc.) regarding the formation of these earliest SMBHs is still uncertain to some large extent.

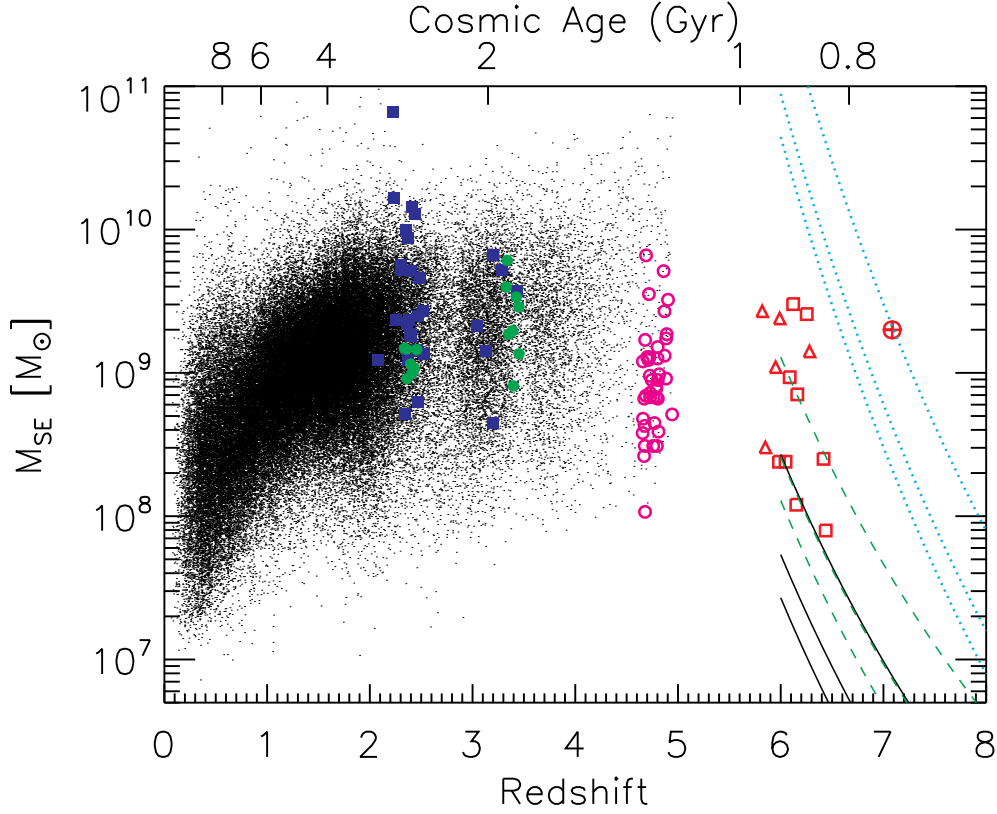


**Figure 9.** A compilation of SE virial mass estimates from different samples of quasars. The black dots are the SE masses for SDSS quasars from Shen et al. (2011), based on  $H\beta$  ( $z < 0.7$ ),  $Mg\ II$  ( $0.7 < z < 1.9$ ) and  $CIV$  ( $z > 1.9$ ). Given the potential caveats of  $CIV$ -based SE masses, near-IR spectroscopy has been undertaken to estimate SE masses for  $z \gtrsim 2$  quasars based on  $H\beta$  and  $Mg\ II$ . The different large symbols are for SE masses based on  $H\beta$  (filled symbols) and  $Mg\ II$  (open symbols) from Shemmer et al. (2004, filled squares), Netzer et al. (2007, filled circles), Trakhtenbrot et al. (2011, open circles), Kurk et al. (2007, open triangles), Willott et al. (2010, open squares), and Mortlock et al. (2011, open circle with cross). Bear in mind the large uncertainty associated with individual SE masses and potential biases. I also show the predicted SMBH growth at  $z > 6$  based on simple, continuous accretion models with constant Eddington ratio  $\lambda$  and radiative efficiency  $\epsilon = 0.1$ , as described in Eqn. (20). The solid lines are Eddington-limited ( $\lambda = 1$ ) growth models from a seed BH at  $z = 20$ ; the dashed lines are  $\lambda = 1$  growth models from a seed BH at  $z = 30$ ; the dotted lines are mildly super-Eddington ( $\lambda = 1.5$ ) growth models from a  $z = 20$  seed BH. For each model I used three seed BH masses,  $M_{\text{seed}} = 10, 20, 100 M_{\odot}$  to accommodate reasonable ranges of seed BH mass from a Pop III star remnant at  $z \sim 20 - 30$ .

While this is not seen as an immediate crisis, there are multiple pathways to make it much easier to grow  $\gtrsim 10^9 M_\odot$  SMBHs at  $z \gtrsim 6$  by boosting either the accretion rate or the seed BH mass (for a recent review, see, e.g., Volonteri 2010; Haiman 2012). These recipes include:

1) supercritical accretion (e.g., Volonteri & Rees 2005) where the accretion rate  $\dot{M}_{\text{BH}}$  greatly exceeds the Eddington limit with a canonical radiative efficiency  $\epsilon = 0.1$ . One possibility is that the radiation is trapped in the accretion flow (e.g., Begelman 1979; Wyithe & Loeb 2012), leading to a very low  $\epsilon$  and hence a much shorter  $e$ -folding time. Note that in such a radiatively inefficient accretion flow (RIAF), the luminosity is still bounded by the Eddington limit;

2) rapid formation of massive ( $\sim 10^3 - 10^5 M_\odot$ ) BH seeds from direct collapse of primordial gas clouds (e.g., Bromm & Loeb 2003; Begelman et al. 2006; Agarwal et al. 2012) or from a hypothetical supermassive star or “quasi-star” (e.g., Shibata & Shapiro 2002; Begelman et al. 2008; Johnson et al. 2012) at high redshift. Supercritical accretion may also be expected in some of these models to grow to the final seed BH mass, which then continue to accrete in the normal way. By increasing  $M_{\text{seed}}$  it requires much less  $e$ -folds to grow to a  $> 10^9 M_\odot$  BH. Another possible route to produce massive BH seeds up to  $\sim 10^3 M_\odot$  is by the runaway collisional growth in a dense star cluster formed in a high-redshift halo (e.g., Omukai et al. 2008).

## 4.2 Quasar Demographics in the Mass-Luminosity Plane

BH mass estimates provide an additional dimension in the physical properties of quasars. The distribution of quasars in the two-dimensional BH mass-luminosity ( $M-L$ ) plane conveys important information about the accretion process of these active SMBHs. The first quasar mass-luminosity plane plot was made by Dibai in the 1970s as mentioned in §2.2. Over the years, such a 2D plot has been repeatedly generated based on increasingly larger quasar samples and improved BH mass estimates (e.g., Wandel et al. 1999; Woo & Urry 2002; Kollmeier et al. 2006; Shen et al. 2008a; Shen & Kelly 2012), and the much better statistics now allows a more detailed and deeper look into this quasar mass-luminosity plane.

In what follows I will mainly focus on the SDSS quasar sample because this is the largest and most homogeneous quasar samples to date. But as emphasized in Shen & Kelly (2012), the SDSS sample only probes the bright-end of the quasar population, and to probe the mass and accretion rate of the bulk of quasars it is necessary to assemble deeper spectroscopic quasar samples (e.g., Kollmeier et al. 2006; Gavignaud et al. 2008; Trump et al. 2009; Nobuta et al. 2012).

Since I have emphasized the distinction between true BH masses and SE mass estimates, I shall use the term “observed” or “measured” to refer to distributions based on SE mass estimates, to distinguish them from “true” distributions. Fig. 10 shows such an *observed* mass-luminosity plane from the same collection of quasars as shown in Fig. 9. Note that these samples are flux-limited to different magnitudes, and several high-redshift samples based on  $H\beta$  or  $\text{Mg II}$  (i.e., large symbols) have a higher flux-limit than the SDSS. I also used slightly different values of bolometric corrections to convert continuum luminosity to bolometric luminosity for those non-

SDSS samples. From this plot we see that the observed distributions of quasars are bounded between constant Eddington ratios  $0.01 \lesssim \lambda \lesssim 1$ , with median values of  $\langle \lambda \rangle \sim 0.1 - 0.3$  for SDSS quasars, and somewhat higher values for the  $z \gtrsim 5$  samples. The dispersion in Eddington ratio in these flux-limited samples is typically  $\sim 0.3$  dex. Similar distributions were observed by, e.g., Kollmeier et al. (2006). However, as demonstrated in, e.g., Shen et al. (2008a); Kelly et al. (2009a, 2010); Shen & Kelly (2012); Kelly & Shen (2013), the observed distribution suffers from the sample flux limit such that low-Eddington ratio objects have a lower probability being selected into the sample, and from the uncertainties and statistical biases of SE masses relative to true masses. The selection effect due to the flux limit and errors in SE masses dramatically modify the intrinsic distribution in the mass-luminosity plane, and must be taken into account when interpreting the observations.

The best approach to tackle these issues is a forward modeling, in which one specifies an underlying distribution of true masses and luminosities and map to the observed mass-luminosity plane by imposing the flux limit and relations between SE virial masses and true masses (e.g., Shen et al. 2008a; Kelly et al. 2009a, 2010). Then the comparisons between model and observed distributions constrain the model parameters with standard Markov Chain Monte Carlo (MCMC) techniques and Bayesian inference. This is a complicated and model-dependent problem, and the best efforts so far are the studies by Shen & Kelly (2012) and Kelly & Shen (2013), building on earlier work by Shen et al. (2008a), Kelly et al. (2009a) and Kelly et al. (2010). Alternatively, Schulze & Wisotzki (2010) developed a maximum likelihood method (also a forward modeling method), which accounts for the effect of the flux limit, but not the errors in SE masses (although the SE errors can be incorporated in such a framework as well). This maximum likelihood method was subsequently adopted in Nobuta et al. (2012) when modeling a faint quasar sample (again, SE errors not taken into account). Most other quasar mass demographic studies, however, did not explicitly model either of these effects (e.g., Greene & Ho 2007; Vestergaard et al. 2008; Vestergaard & Osmer 2009).

Shen & Kelly (2012) used forward modeling with Bayesian inference to model the observed distribution in the mass-luminosity plane of SDSS quasars, taking into account a possible luminosity-dependent bias (i.e.,  $\beta \neq 0$ , see §3.3.2) to be constrained by the data. The flux limit of the SDSS sample is taken into account using published selection functions of SDSS quasars (Richards et al. 2006a). Based on this approach, Shen & Kelly (2012) found evidence for a non-zero  $\beta$ , although the constraints on  $\beta$  are weak and cannot rule out a null value. Kelly & Shen (2013) used a more flexible model parametrization to describe the underlying true distributions (in BH mass and Eddington ratio), but fixed  $\beta = 0$  to test how sensitively the results in Shen & Kelly (2012) depend on different model parameterizations. They found that the main conclusions are generally consistent, although the results in the latter work are less constrained than in the former, due to the more flexible models. Both studies revealed that based on the SDSS quasar sample alone, it is difficult to constrain the BHMF to better than a factor of a few at most redshifts. This is both because the SDSS sample only probes the tip of the active SMBH population at high- $z$ , and to a larger extent, because the errors of SE masses are poorly understood. However, there are some solid conclusions from the two studies:



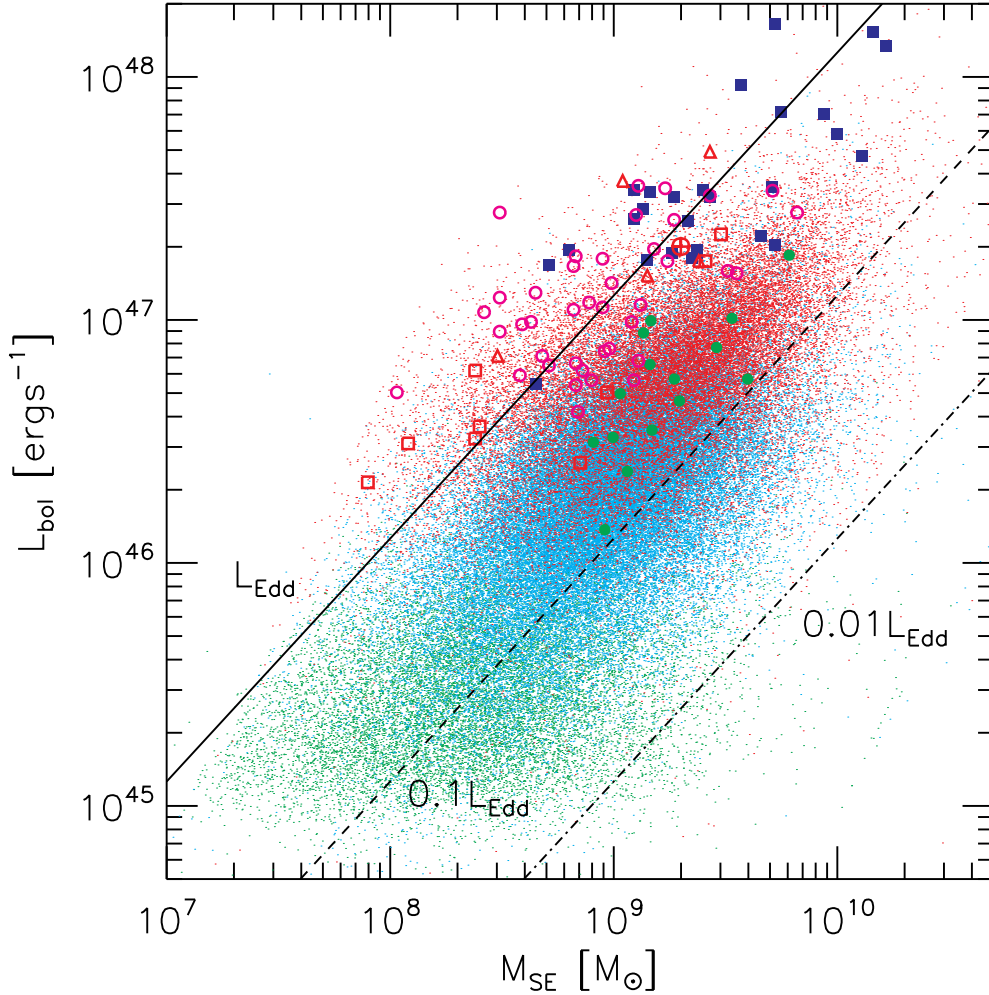


**Figure 10.** The observed quasar mass-luminosity plane based on SE masses for quasars in a wide range of redshifts ( $0 < z \lesssim 7$ ) from the samples compiled in Fig. 9. The dots are from the SDSS sample in Shen et al. (2011), for quasars at  $z < 0.7$  ( $H\beta$ -based SE masses; green),  $0.7 < z < 1.9$  ( $Mg\ II$ -based SE masses; cyan), and  $1.9 < z < 5$  (CIV-based SE masses; red). The large symbols are from various  $z \gtrsim 2$  samples using  $H\beta$  or  $Mg\ II$ -based SE masses. I have used slightly different bolometric corrections for these non-SDSS samples from those used in the original papers. The SDSS quasars have Eddington ratios  $0.01 \lesssim \lambda \lesssim 1$  with a mean value of  $\langle \lambda \rangle \sim 0.1 - 0.3$ , while the other high- $z$  samples have even higher Eddington ratios. Given the flux-limited nature of all these samples and the errors in SE masses, the *observed* Eddington ratio distribution is highly biased relative to the intrinsic distribution (see §4.2 for details).

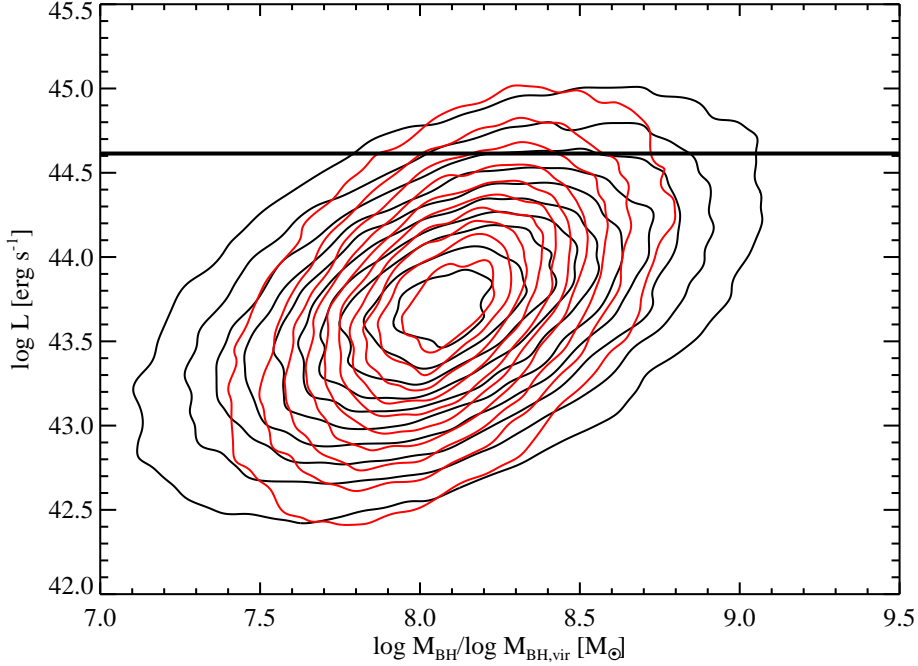


**Figure 11.** The simulated mass-luminosity plane at  $z = 0.6$  based on the modeling of SDSS quasars in Shen & Kelly (2012), which extends below the flux limit (the black horizontal line). The  $y$ -axis plots the restframe  $2500\text{\AA}$  monochromatic luminosity, and the bolometric luminosity is  $L_{\text{bol}} \sim 5L$ . The red contour is the distribution based on *true* BH masses and is determined by the model BHMF and Eddington ratio distribution in Shen & Kelly (2012). The black contour is the distribution based on  $H\beta$  SE BH masses. The flux limit only selects the most luminous objects into the SDSS sample (which are closer to the Eddington limit), and the distribution based on SE virial BH masses is flatter than the one based on true masses due to both the scatter  $\sigma_{ml}$  and a non-zero  $\beta \sim 0.2$  for this redshift bin (see §3.3.2 and Shen & Kelly 2012).

1. The *observed* distribution in the mass-luminosity plane is quite different from the intrinsic distribution, due to the flux limit and uncertainties in SE masses. This is demonstrated in Fig. 11, which shows a quasar  $M - L$  plane at  $z = 0.6$  based on the modeling of SDSS quasars by Shen & Kelly (2012). In this plot luminosity  $L$  is the restframe  $2500\text{\AA}$  monochromatic luminosity, and the bolometric luminosity is  $L_{\text{bol}} \sim 5L$ . The red contours are the *true* distribution of quasars, while the black contours are the *measured* distribution based on  $H\beta$  SE virial masses. The black horizontal line indicates the flux limit of the sample, hence only objects above this line would be selected in the SDSS sample, which form the *observed* distribution. The flux limit only selects the most luminous objects into the SDSS sample, missing the bulk of low Eddington ratio objects; even the highest mass bins are incomplete due to the flux limit. The distribution based on SE virial BH masses is flatter

than the one based on true masses due to the scatter and luminosity-dependent bias of these SE masses.

For the *observed* distribution based on SE masses, there are fewer objects towards larger SE masses and luminosity. This was interpreted as the lack of massive black holes accreting at high Eddington ratios, or the so-called “sub-Eddington boundary” claimed by Steinhardt & Elvis (2010a). However, such a feature is caused by the flux limit and errors in SE masses, and there is no evidence that high-mass quasars on average accrete at lower Eddington ratios, not for broad-line objects at least<sup>10</sup>. This conclusion seems to be robust against different model parameterizations of the underlying true distributions in the forward modeling approach (Kelly & Shen 2013). Of course here I am assuming no systematic biases in these FWHM-based SE masses measured in Shen et al. (2011). It is possible that  $\sigma_{\text{line}}$ -based SE masses are more reliable, in which case there would be a “rotation” in the mass-luminosity plane using  $\sigma_{\text{line}}$ -based SE masses, as discussed in §3.1.3. This also tends to reduce this “sub-Eddington boundary” in the observed plane (e.g., Rafiee & Hall 2011a,b), but a full modeling taking into account both the flux limit and SE mass errors is yet to be performed with  $\sigma_{\text{line}}$ -based SE masses (i.e., the interpretation by Rafiee & Hall is still based on “observed” rather than true distributions).

2. The intrinsic Eddington ratio distribution at fixed true mass is broader ( $\sim 0.4$  dex) than the *observed* Eddington ratio distribution in flux-limited samples ( $\lesssim 0.3$  dex), and the mean Eddington ratio in the flux-limited samples based on SE masses is higher<sup>11</sup> than the mean Eddington ratio for all active SMBHs (most of which are not detected). This is consistent with earlier studies by Shen et al. (2008a) and Kelly et al. (2010). Some deeper spectroscopic surveys indeed start to find these lower Eddington ratio objects (e.g., Babić et al. 2007; Gavignaud et al. 2008; Nobuta et al. 2012), and are consistent with the model-extrapolated distributions from Shen & Kelly (2012) and Kelly & Shen (2013); however, since in general these deep data are noisier and the selection function is less well quantified than SDSS, care must be paid when inferring the dispersion in Eddington ratios for these faint quasars.

The next step to utilize this quasar mass-luminosity plane is to measure the abundance of quasars in this plane, and study its redshift evolution. This is a much more powerful way to study the cosmic evolution of quasars than traditional 1D distribution functions such as the luminosity function (LF) and the quasar BHMF.

I demonstrate the power of the mass-luminosity plane in quasar demographic studies in Fig. 12. This is the same simulated, *true* quasar  $M - L$  plane at  $z = 0.6$  as in Fig. 11, using the models in Shen & Kelly (2012) constrained using SDSS quasars. The 2D density (i.e., abundance)

<sup>10</sup>There could be a significant population of high-mass, non-broad-line AGNs accreting at low Eddington ratios, possibly via a different accretion mode than broad line quasars.

<sup>11</sup>These SE masses are on average overestimated due to the luminosity-dependent bias discussed in §3.3.2, which tends to underestimate the true Eddington ratios. But the mean observed Eddington ratio based on SE masses of the flux-limited sample is still higher than the mean value for all quasars extending below the flux limit (see fig. 19 of Shen & Kelly 2012).

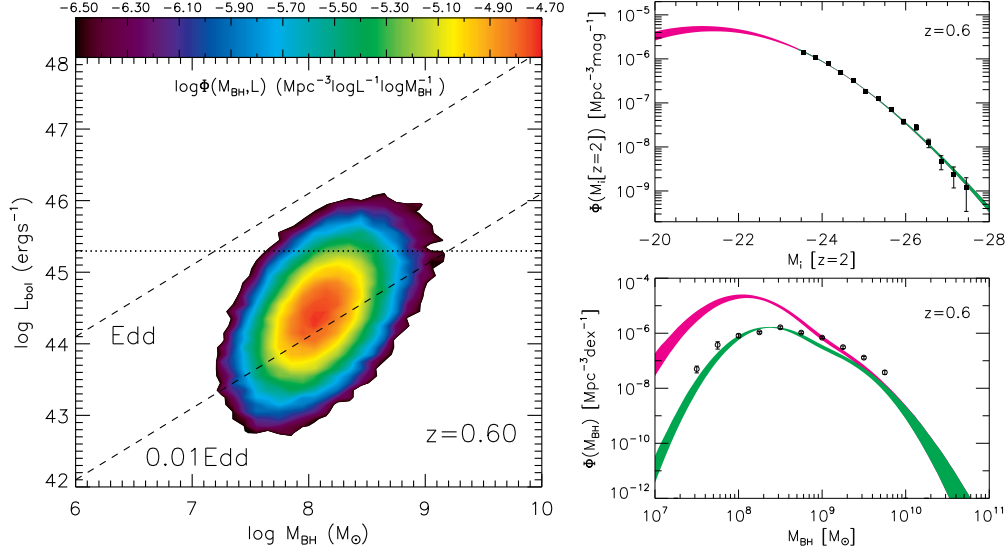


**Figure 12.** An example of the forward modeling of quasar demographics in the mass-luminosity plane by Shen & Kelly (2012), modeled at  $z = 0.6$ . *Left:* The simulated mass-luminosity plane (with *true* BH masses), which extends below the SDSS flux limit (the black horizontal line). Shown here is the comoving number density map  $[\Phi(M_{\text{BH}}, L)]$ , where only regions with  $\Phi(M_{\text{BH}}, L) > 10^{-6.5} \text{ Mpc}^{-3} \log L^{-1} \log M_{\text{BH}}^{-1}$  are shown. The two diagonal lines indicate constant Eddington ratios of 1 and 0.01. The flux limit only selects the most luminous objects into the SDSS sample. *Right:* Projections of the 2D distribution onto the luminosity and BH mass axes, i.e., the LF (upper right) and BHMF (bottom right) of quasars at  $z = 0.6$ . The points are binned observational data and the lines are best-fit models: the magenta lines show the results for all broad-line quasars (corrected for the flux limit) and the green lines show those for the flux-limited sample. The thickness of the lines indicates the  $1\sigma$  model uncertainty. I have used the *i*-band absolute magnitude instead of bolometric luminosity in presenting the LF, and I have also taken into account the difference between true BH masses (colored lines) and SE virial BH masses (points). This forward-modeling framework accounts for the selection incompleteness in BH mass due to the flux limit, and the uncertainties in SE virial BH mass estimates, and can constrain the 2D distribution down to  $\sim 3$  magnitudes fainter than the flux limit (Shen & Kelly 2012). However, to make more robust constraints at the faint end, deeper quasar samples are highly desirable.

The 2D distribution of quasars offers significantly more information on the evolution of quasars than 1D distributions (i.e., LF or BHMF) alone. Specifically if we focus on snapshots of the mass-luminosity plane in short time intervals (e.g., shorter than typical quasar lifetime), then objects will move along certain evolutionary tracks in the plane, determined by the evolution of Eddington ratio (possibly also coupled with the change of the radiative efficiency as accretion rate evolves). This evolution in the mass-luminosity plane can be modeled in great detail, and compared with either analytical models or numerical simulations of SMBH growth. This is somewhat similar to the simple arguments in the quasar LF literature (such as the “pure luminosity evolution” model), but the diagnostic capabilities of the mass-luminosity plane would be far more powerful and self-consistent in terms of SMBH growth and light curve evolution.

of quasars in this plane is shown in the color-coded contours. The traditional LF and BHMF (shown in the right panels) are then just the projection onto each axis. In the right panels I also demonstrate the differences between using true BH masses and SE virial masses, as well as the effect of the sample flux limit. It is clear from this demonstration that the 1D distribution functions lose information by collapsing on one dimension, and a better way to study the demography of quasars is to measure their abundance in 2D, since the mass and luminosity of a quasar are physically connected by the Eddington ratio. The ultimate goal is to study the evolution of the quasar density in the  $M-L$  plane as a function of time. Recent studies have started to work in this direction (e.g., Shen & Kelly 2012; Kelly & Shen 2013), although deeper quasar samples and a better understanding of SE mass errors are needed to utilize the full power of the  $M-L$  plane.

To summarize, the quasar mass-luminosity plane has great potential in studying quasar evolution, and efforts have been underway to investigate this plane in detail (e.g., Steinhardt & Elvis 2010a,b; Steinhardt et al. 2011; Steinhardt & Elvis 2011; Shen & Kelly 2012; Kelly & Shen 2013). However, it should always be kept in mind that the “observed” distribution in the  $M-L$  plane is *not* the true distribution. I strongly discourage direct interpretations of the observed distributions based on SE masses and flux-limited data, which can easily lead to superficial or even spurious results.

### 4.3 Evolution of BH-Bulge Scaling Relations

Another important application of SE virial mass estimators is to study the  $M_{\text{BH}}$ -host scaling relations in broad line AGNs, and to probe the evolution of these relations at high redshift. Measuring the  $M_{\text{BH}}$ -host relations in low redshift quasars and AGNs has been done using both RM masses and SE masses (e.g., Laor 1998; Greene & Ho 2006; Bentz et al. 2009c; Xiao et al. 2011). Assuming some virial coefficient  $\langle f \rangle$ , these studies were able to add active objects in these scaling relations and extend the dynamic range in BH mass.

In the past a few years, there have been a huge amount of effort to quantify the evolution of these scaling relations up to  $z \sim 6$ , by measuring host properties in broad-line quasars. Some studies directly measure the galaxy properties by decomposing the quasar and galaxy light in either imaging or spectroscopic data (e.g., Treu et al. 2004; Peng et al. 2006a,b; Woo et al. 2006; Treu et al. 2007; Woo et al. 2008; Shen et al. 2008b; Jahnke et al. 2009; McLeod & Bechtold 2009; Decarli et al. 2010; Merloni et al. 2010; Bennert et al. 2010; Cisternas et al. 2011; Targett et al. 2012); other studies use indirect methods to infer galaxy properties, such as using the narrow emission line width to infer bulge velocity dispersion (e.g., Shields et al. 2003, 2006; Salviander et al. 2007; Salviander & Shields 2012). Molecular gas (using CO tracers) has also been detected in the hosts of  $z \sim 6$  quasars, allowing rough estimates on the host dynamical mass of these highest redshift quasars (e.g., Walter et al. 2004; Wang et al. 2010, and references therein). In all cases the BH masses were estimated using the SE methods based on different broad emission lines. With a few exceptions, most of these studies claim an excess in BH mass relative to bulge properties either in the  $M_{\text{BH}} - \sigma_*$  relation or in the  $M_{\text{BH}} - M_{\text{bulge}}/L_{\text{bulge}}$  relation, and advocate a scenario where BH growth precedes spheroid assembly.

It is worth noting that measuring host galaxy properties of Type 1 AGNs could be challenging, and systematic biases may arise when measuring the stellar velocity dispersion from spectra (e.g., Bennert et al. 2011), or host luminosities from image decomposing (e.g., Kim et al. 2008; Simmons & Urry 2008). Conversions from measurables (such as host luminosity) to derived quantities (such as stellar mass) are also likely subject to systematics, especially for low-quality data. Thus careful treatments are required to derive unbiased host measurements.

On the other hand, it is also worrisome that the errors in SE BH mass estimates may affect the observed offset in the BH scaling relations at high-redshift. As discussed extensively in §3, there are both physical and practical concerns that the applications of locally-calibrated SE estimators to high-redshift quasars may cause systematic biases. Even if the extrapolations are valid, the luminosity-dependent bias discussed in §3.3.2 may still lead to an average overestimation of quasar BH masses in flux-limited surveys. Shen & Kelly (2010) studied the impact of the luminosity-dependent bias on flux-limited quasar samples, and found an “observed” BH mass excess of  $\sim 0.2 - 0.3$  dex for  $L_{\text{bol}} \gtrsim 10^{46}$  erg s $^{-1}$  with a reasonable value of  $\sigma'_l = 0.4$  dex (see §3.3.2 for details). This sample bias using SE mass estimates becomes larger (smaller) at higher (lower) threshold quasar luminosities.

Another statistical bias was pointed out by Lauer et al. (2007), which is at work even if there is no error in BH mass estimates. The basic idea is that since there is an intrinsic scatter between BH mass and bulge properties ( $\sim 0.3$  dex for the local sample), and since the distribution functions in BH mass and galaxy properties are expected to be bottom-heavy, a statistical excess (bias) in the average BH mass relative to bulge properties arises when the sample is selected based on BH mass (or based on quasar luminosity, assuming the Eddington ratio is constant). This is similar to the Malmquist-type bias discussed in §3.3.1. One can work out (e.g., Lauer et al. 2007; Shen & Kelly 2010) that the BH mass offset introduced by this bias depends on the slope of the galaxy distribution function, as well as the scatter in the BH-host scaling relations. For simple power-law models of the galaxy distribution function on property  $S$  with a slope  $\gamma_s$ , and lognormal scatter  $\sigma_\mu$  at fixed galaxy property  $S$ , this bias takes a similar form as the Malmquist-type bias in §3.3.1:

$$\Delta \log M_{\text{BH,Lauer}} = -\ln(10)\gamma_s\sigma_\mu^2/C, \quad (21)$$

where  $C$  is the coefficient of the mean BH-host property ( $S$ ) scaling relation  $\log M_{\text{BH}} = C \log S + C'$ . Thus if the intrinsic scatter in the BH-host scaling relations increases with redshift, then this statistical bias alone can contribute a significant amount to the observed BH mass offset in the high-redshift samples (e.g., Merloni et al. 2010). A larger intrinsic scatter in these scaling relations at high redshift is expected, if the tightness of the local BH-host scaling relations is mainly established via the hierarchical merging of less-correlated BH-host systems at higher redshift (e.g., Peng 2007; Hirschmann et al. 2010; Jahnke & Macció 2011). The real situation is of course more complicated, and one must consider a realistic Eddington ratio distribution at fixed BH mass and the effect of the flux limit. There could also be other factors that may complicate the usage of AGNs to probe the evolution of these BH-host scaling relations, as discussed in detail in Schulze & Wisotzki (2011). But overall a BH mass excess due to the Lauer et al. bias is expected when select on quasar luminosity. An interesting corollary is that a deficit in BH mass is expected if the sample is selected based on galaxy properties. This may explain the findings

that high-redshift submillimeter galaxies (SMGs) tend to have on average smaller BHs relative to expectations from local BH-host scaling relations (e.g., Alexander et al. 2008).

The Lauer et al. bias caused by the intrinsic scatter in BH-host scaling relations works independently with the luminosity-dependent bias caused by errors in SE masses, so together they can contribute a substantial (or even full) amount of the observed BH mass excess at high redshift (e.g., Shen & Kelly 2010). Both biases are generally worse for samples with a higher luminosity threshold given the curvature in the underlying distribution function<sup>12</sup>, thus higher- $z$  samples with higher intrinsic AGN luminosities will have larger BH mass biases, leading to an apparent evolution. There are several samples that are probing similar luminosities as the local RM AGN sample (e.g., Woo et al. 2006). Since the SE mass estimators were calibrated on the local  $M_{\text{BH}} - \sigma_*$  relation using the RM AGN sample, one argument often made is that both biases should be calibrated away for the high- $z$  sample with similar AGN luminosities. This argument is flawed, however, because the local RM AGN sample is heterogeneous and is not sampling uniformly from the underlying BH/galaxy distribution functions, while the high- $z$  sample usually is sampling uniformly from the underlying distributions – this is exactly why both biases will arise for the high- $z$  samples. The only exception that might work is to compare two quasar samples at two different redshifts with the same luminosity threshold, where the predicted BH mass biases should be of the same amount, and see if there is evolution in the average host properties. But even in this case it requires that the underlying distributions (slope and scatter) and measurement systematics are the same for both the low- $z$  and high- $z$  samples. Proper simulations that take into account the measurement systematics (in both BH mass and host properties) and underlying distributions should be performed to verify the interpretations upon the observations.

To summarize, there might be true evolutions in the BH-host scaling relations<sup>13</sup>, but the current observations are inconclusive, due to the unknown systematics in the BH mass and host galaxy measurements. Better understandings of these systematics, the selection effects, as well as theoretical priors are all needed to probe the evolution of these scaling relations, and such efforts have been underway (e.g., Croton 2006; Robertson et al. 2006; Lauer et al. 2007; Hopkins et al. 2007; Di Matteo et al. 2008; Booth & Schaye 2009; Shankar et al. 2009; Shen & Kelly 2010; Hirschmann et al. 2010; Schulze & Wisotzki 2011; Jahnke & Macció 2011; Portinari et al. 2012; Salviander & Shields 2012; Zhang et al. 2012).

## 5. Summary and Future Perspectives

To conclude, there have been considerable progress over the past several decades on the development of BH weighing methods for quasars. We now have a working technique based on

---

<sup>12</sup>This is not always the case. If the scatter ( $\sigma_\mu, \sigma'_l$ ) increases at the low-mass end, then both biases could be worse at the low-mass/luminosity end.

<sup>13</sup>If the mass and velocity dispersion of galaxies bear any resemblance to the virial mass ( $M_{\text{h,vir}}$ ) and virial velocity ( $V_{\text{h,vir}}$ ) of their host dark matter halos, then one of the two relations,  $M_{\text{BH}} - \sigma_*$  and  $M_{\text{BH}} - M_{\text{bulge}}$ , must evolve since the  $M_{\text{h,vir}} - V_{\text{h,vir}}$  relation is redshift-dependent.

reverberation mapping of broad line AGNs that can measure active virial BH masses with an accuracy of a factor of a few ( $\sim 0.5$  dex). Rooted in the RM technique, efficient SE virial mass estimators have been developed to measure BH mass for large statistical samples of broad line quasars based on single-epoch spectroscopy. These methods greatly facilitate quasar studies in the era of modern, large-scale spectroscopic surveys.

However, there are outstanding issues regarding the reliability of these virial (RM or SE) mass estimators, and consequences of their significant uncertainties, which is the focus of this review. Specifically I have the following highlighting remarks.

- There are genuine concerns that the current RM sample does not represent the whole quasar/AGN population, and the limited sample size and luminosity/redshift ranges of the RM sample, as well as the poorly understood BLR structure and dynamics, may impact the applicability of these locally-calibrated SE relations to high- $z$  and/or high-luminosity quasars (§3.1). Due to limitations of the current RM sample and the uncertainty in the average virial coefficient  $\langle f \rangle$ , systematic biases on the order of a factor of a few are likely present due to these physical caveats.
- Even when the extrapolation of these SE estimators to high- $z$  quasars is justified, rigorous statistical biases will arise from the uncertainties (scatter) in these SE masses (§3.3). In particular I demonstrated the conceptual difference between errors in SE masses and the distribution of SE masses within restricted luminosity ranges. Since luminosity is used in the estimation of SE masses, the variance in SE mass is reduced when luminosity is constrained. I also derived the luminosity-dependent bias (e.g., Shen et al. 2008a; Shen & Kelly 2010, 2012) that at fixed true mass, the SE masses are over(under)-estimated in the mean when luminosity is higher (lower) than the mean luminosity at this fixed true mass, due to the stochastic variations between luminosity and line width that contribute to the uncertainty of SE masses. Simple simulations were performed to demonstrate these effects, and suggest that sample biases on the order of a factor of a few are present in flux-limited bright quasar sample. Thus these error-induced biases are *as significant as* the unknown systematic biases in SE masses, and cannot be ignored. More importantly, even when we eliminate all systematic biases (zero-point uncertainty) of these SE estimators in the future, these error-induced statistical biases will largely remain given the imperfect nature of these estimators. The formalism in §3.3.2 provides guidance on how to quantify these error-induced sample biases with simulations.
- Properly accounting for the selection effect due to the sample flux limit, and statistical biases arising from errors in SE masses, are crucial to interpreting the observed distributions of quasars in statistical samples (§4). I discussed how the “observed” distributions of BH mass and Eddington ratio for threshold data and with SE masses differ from the “true” distributions (§4.2), and cautioned on some recent claims based directly on the observed distributions. I further commented on the impact of the error-induced biases in SE masses on studies of the evolution of the BH-host scaling relations (§4.3), and concluded that the current observations are inconclusive for the claimed evolution.



Looking forward, there is an urgent need to expand the current RM sample with lag measurements, and, to acquire exquisite (velocity-resolved) RM data to utilize the full power of this technique. Only with a substantially larger RM sample that properly probes the AGN parameter space, and with a much better understanding of the BLR geometry and dynamics (for different lines) based on these RM data and ancillary data, can we improve these virial BH mass estimators further. Since resource-wise, RM is a consuming exercise, it would be interesting to explore the possibilities of more efficient RM with wide-field multi-object imaging and spectroscopy, as well as dedicated facilities for single-object-mode monitoring.

There are a few recent innovative proposals regarding RM that are worth mentioning. Zu et al. (2011) proposed an alternative method to measure RM lags, by fitting the observed continuum and emission line light curves with recently-developed statistical models to describe quasar variability (e.g., the “damped random walk” model developed by Kelly et al. 2009b; Kozłowski et al. 2010). Compared with the traditional cross-correlation method in measuring RM lags (e.g., Gaskell & Peterson 1987), this new method can improve lag measurements by simultaneously fitting multiple lines and quantifying error correlations. In addition, there have been efforts to build dynamical BLR models to directly model the RM light curves in the time domain (e.g., Brewer et al. 2011; Pancoast et al. 2012); such forward modeling (as discussed in, e.g., Netzer & Peterson 1997) can in principle provide direct constraints on the geometry of the BLR and the mass of the BH, and so it is worthwhile to explore its potential further. Finally, alternative strategies in RM experiments with no or few spectroscopic data (e.g., Haas et al. 2011; Chelouche & Daniel 2012; Fine et al. 2012), while not as good and reliable as traditional spectroscopic RM, may speed up the process of probing the diversity of AGN parameters in the context of RM.

## Acknowledgements

I thank all my collaborators and colleagues for many stimulating and enlightening discussions on this subject over the past a few years. In writing this review I benefited a lot from inspiring conversations with and/or feedback from Brandon Kelly, Luis Ho, Brad Peterson, Gordon Richards, Roberto Assef, Aaron Barth, Neil Brandt, Kelly Denney, Jenny Greene, Pat Hall, Zoltan Haiman, Chris Kochanek, Juna Kollmeier, Tod Lauer, Xin Liu, Youjun Lu, Chien Peng, Alireza Rafiee, Andreas Schulze, Charles Steinhardt, Michael Strauss, Benny Trakhtenbrot, Scott Tremaine, Marianne Vestergaard, David Weinberg, Jong-Hak Woo, and Qingjuan Yu. I acknowledge support from the Carnegie Observatories through a Hubble Fellowship from Space Telescope Science Institute. Support for Program number HST-HF-51314.01-A was provided by NASA through a Hubble Fellowship grant from the Space Telescope Science Institute, which is operated by the Association of Universities for Research in Astronomy, Incorporated, under NASA contract NAS5-26555.

## References

Abramowicz, M. A., & Fragile, P. C. 2013, Living Reviews in Relativity, arXiv:1104.5499

- Agarwal, B., et al. 2012, MNRAS, 425, 2854  
Akritas, M. G., & Bershadsky, M. A. 1996, ApJ, 470, 706  
Alexander, D. M., Hickox, R. C. 2012, NewAR, 56, 93  
Alexander, D. M., et al. 2008, AJ, 135, 1968  
Aller, M. C., Richstone, D. O. 2007, ApJ, 665, 120  
Assef, R. J., et al. 2011, ApJ, 742, 93  
Assef, R. J., et al. 2012, ApJ, 753, L2  
Babić, A., et al. 2007, A&A, 474, 755  
Bachev, R., et al. 2004, ApJ, 617, 171  
Bahcall, J. N., Kozlovsky, B.-Z., & Salpeter, E. E. 1972, ApJ, 171, 467  
Baldwin, J. A. 1977, ApJ, 214, 679  
Baskin, A., & Laor, A. 2005, MNRAS, 356, 1029  
Begelman, M. C. 1979, MNRAS, 187, 237  
Begelman, M. C., Rossi, E. M., & Armitage, P. J. 2008, MNRAS, 387, 1649  
Begelman, M. C., Volonteri, M., & Rees, M. J. 2006, MNRAS, 370, 289  
Bennert, V. N., et al. 2010, ApJ, 708, 1507  
Bennert, V. N., Auger, M. W., Treu, T., Woo, J.-H., & Malkan, M. A. 2011, ApJ, 726, 59  
Bentz, M. C., et al. 2006, ApJ, 644, 133  
Bentz, M. C., Peterson, B. M., Netzer, H., Pogge, R. W., & Vestergaard, M. 2009a, ApJ, 697, 160  
Bentz, M. C., et al. 2009b, ApJ, 705, 199  
Bentz, M. C., et al. 2009c, ApJ, 694, L166  
Bentz, M. C., et al. 2010, ApJ, 720, L46  
Blandford, R. D., & McKee, C. F. 1982, ApJ, 255, 419  
Bochkarev, N. G., & Gaskell, C. M. 2009, Astronomy Letters, 35, 287  
Booth, C. M., & Schaye, J. 2009, MNRAS, 398, 53  
Boroson, T. A., & Green, R. F. 1992, ApJS, 80, 109  
Brewer, B. J. 2011, ApJ, 733, L33  
Bromm, V., & Loeb, A. 2003, ApJ, 596, 34  
Bromm, V., & Yoshida, N. 2011, ARA&A, 49, 373  
Bromm, V., Yoshida, N., Hernquist, L., & McKee, C. F. 2009, Nature, 459, 49  
Calderone, G., Ghisellini, G., Colpi, M., & Dotti, M. 2012, arXiv:1212.1181  
Chelouche, D., & Daniel, E. 2012, ApJ, 747, 62  
Chen, K., Halpern, J. P., & Filippenko, A. V. 1989, ApJ, 339, 742  
Cisternas, M., et al. 2011, ApJ, 741, L11  
Collin, S., Kawaguchi, T., Peterson, B. M., & Vestergaard, M. 2006, A&A, 456, 75  
Collin-Souffrin, S., Dyson, J. E., McDowell, J. C., & Perry, J. J. 1988, MNRAS, 232, 539  
Croom, S. M. 2011, ApJ, 736, 161  
Croton, D. J., 2006, MNRAS, 369, 1808  
Czerny, B., & Nikolajuk, M. 2010, Memorie della Societ à Astronomica Italiana, 81, 281  
Czerny, B., et al. 2012, arXiv:1212.0472  
Di Matteo, T., Colberg, J., Springel, V., Hernquist, L., & Sijacki, D. 2008, ApJ, 676, 33  
Di Matteo, T., Springel, V., & Hernquist, L. 2005, Nature, 433, 604  
Dai, X., et al. 2010, ApJ, 709, 278  
Davidson, K. 1972, ApJ, 171, 213

- Davidson, K., & Netzer, H. 1979, *Rev. Mod. Phys.*, 51, 715
- Davies, R. I. 2006, *ApJ*, 646, 754
- Davis, S. W., & Laor, A. 2011, *ApJ*, 728, 98
- Decarli, R., Dotti, M., Fontana, M., & Haardt, F. 2008b, *MNRAS*, 386, L15
- Decarli, R., Labita, M., Treves, A., & Falomo, R. 2008a, *MNRAS*, 387, 1237
- Decarli, R., et al. 2010, *MNRAS*, 402, 2453
- Denney, K. D. 2012, *ApJ*, 759, 44
- Denney, K. D., et al. 2009b, *ApJ*, 692, 246
- Denney, K. D., et al. 2009a, *ApJ*, 704, L80
- Dibai, E. A. 1977, *Soviet Astronomy Letters*, 3, 1
- Dibai, E. A. 1980, *Soviet Astronomy*, 24, 389
- Dibai, E. A. 1984, *Soviet Astronomy*, 28, 245
- Dietrich, M., Appenzeller, I., Vestergaard, M., & Wagner, S. J. 2002, *ApJ*, 564, 581
- Dietrich, M., & Hamann, F. 2004, *ApJ*, 611, 761
- Dietrich, M., Mathur, S., Grupe, D., & Komossa, S. 2009, *ApJ*, 696, 1998
- Eddington, A. S. 1913, *MNRAS*, 73, 359
- Elvis, M. 2000, *ApJ*, 545, 63
- Elvis, M., Risaliti, G., & Zamorani, G. 2002, *ApJ*, 565, L75
- Eracleous, M., Livio, M., Halpern, J. P., & Storchi-Bergmann, T. 1995, *ApJ*, 438, 610
- Eracleous, M., & Halpern, J. P. 1994, *ApJS*, 90, 1
- Everett, J. E. 2005, *ApJ*, 631, 689
- Fabian, A. C. 1999, *MNRAS*, 308, 39
- Fan, X., et al. 2001, *AJ*, 122, 2833
- Ferrarese, L., & Ford, H. 2005, *Space Science Reviews*, 116, 523
- Ferrarese, L., & Merritt, D. 2000, *ApJ*, 539, L9
- Fine, S., Jarvis, M. J., & Mauch, T. 2011, *MNRAS*, 412, 213
- Fine, S., et al. 2008, *MNRAS*, 390, 1413
- Fine, S., et al. 2010, *MNRAS*, 409, 591
- Fine, S., et al. 2012, *MNRAS*, 427, 2701
- Gaskell, C. M. 1982, *ApJ*, 263, 79
- Gaskell, C. M. 1988, *ApJ*, 325, 114
- Gaskell, C. M. 2009, *NewAR*, 53, 140
- Gaskell, C. M., & Peterson, B. M. 1987, *ApJS*, 65, 1
- Gavignaud, I., et al. 2008, *A&A*, 492, 637
- Gebhardt, K., et al. 2000, *ApJ*, 539, L13
- Ghisellini, G., et al. 2010, *MNRAS*, 405, 387
- Glikman, E., et al. 2007, *ApJ*, 667, 673
- Goad, M. R., Korista, K. T., & Ruff, A. J. 2012, *MNRAS*, 426, 3086
- Graham, A. W. 2008, *PASA*, 25, 167
- Graham, A. W., Erwin, P., Caon, N., & Trujillo, I. 2001, *ApJ*, 563, L11
- Graham, A. W., & Li, I.-H. 2009, *ApJ*, 698, 812
- Graham, A. W., Onken, C. A., Athanassoula, E., & Combes, F. 2011, *MNRAS*, 412, 2211
- Grandi, S. A. 1982, *ApJ*, 255, 25
- Greene, J. E., & Ho, L. C. 2005, *ApJ*, 630, 122

- Greene, J. E., & Ho, L. C. 2006, *ApJ*, 641, L21  
Greene, J. E., & Ho, L. C. 2007, *ApJ*, 667, 131  
Greene, J. E., Ho, L. C., & Barth, A. J. 2008, *ApJ*, 688, 159  
Greene, J. E., Peng, C. Y., & Ludwig, R. R. 2010a, *ApJ*, 709, 937  
Greene, J. E., et al. 2010b, *ApJ*, 721, 26  
Grier, C. J., et al. 2013, *ApJ*, 764, 47  
Guerras, E., et al. 2013, *ApJ*, in press, arXiv:1207.2042  
Gültekin, K., et al. 2009, *ApJ*, 698, 198  
Haiman, Z., & Cen, R. 2002, *ApJ*, 578, 702  
Haiman, Z., & Loeb, A. 2001, *ApJ*, 552, 459  
Haiman, Z. 2012, arXiv:1203.6075  
Haas, M., et al. 2011, *A&A*, 535, 73  
Hicks, E. K. S., & Malkan, M. A. 2008, *ApJS*, 174, 31  
Hirschmann, M., et al. 2010, *MNRAS*, 407, 1016  
Ho, L. C. 1999, in *Observational Evidence for Black Holes in the Universe*, ed. S. K. Chakrabarti (Dordrecht: Kluwer), 157  
Ho, L. C., Goldoni, P., Dong, X.-B., Greene, J. E., & Ponti, G. 2012, *ApJ*, 754, 11  
Hopkins, P. F., Hernquist, L., Cox, T. J., Robertson, B., & Krause, E. 2007, *ApJ*, 669, 45  
Horne, K., Peterson, B. M., Collier, S. J., & Netzer, H. 2004, *PASP*, 116, 465  
Hosokawa, T., Omukai, K., Yoshida, N., & Yorke, H. W. 2011, *Science*, 334, 1250  
Hoyle, F., & Fowler, W. A. 1963, *Nature*, 197, 533  
Hu, J. 2008, *MNRAS*, 386, 2242  
Hu, J. 2009, *MNRAS*, arXiv:0908.2028  
Irwin, M. J., Webster, R. L., Hewett, P. C., Corrigan, R. T., Jędrzejewski, R. I. 1989, *AJ*, 98, 1989  
Jahnke, K., et al. 2009, *ApJ*, 706, L215  
Jahnke, K., & Macciò, A. V. 2011, *ApJ*, 734, 92  
Jarvis, M. J., McLure, R. J. 2006, *MNRAS*, 369, 182  
Jiang, L., et al. 2007, *AJ*, 134, 1150  
Johnson, J. L., Whalen, D. J., Fryer, C. L., & Li, H. 2012, *ApJ*, 750, 66  
Kaspi, S., et al. 2007, *ApJ*, 659, 997  
Kaspi, S., et al. 2005, *ApJ*, 629, 61  
Kaspi, S., Smith, P. S., Netzer, H., Maoz, D., Jannuzi, B. T., & Giveon, U. 2000, *ApJ*, 533, 631  
Keeton, C. R., Kuhlen, M., & Haiman, Z. 2005, *ApJ*, 621, 559  
Kelly, B. C. 2007, *ApJ*, 665, 1489  
Kelly, B. C., & Bechtold, J. 2007, *ApJS*, 168, 1  
Kelly, B. C., Bechtold, J., & Siemiginowska, A. 2009b, *ApJ*, 698, 895  
Kelly, B. C. & Shen, Y. 2013, *ApJ*, 764, 45  
Kelly, B. C., Vestergaard, M., & Fan, X. 2009a, *ApJ*, 692, 1388  
Kelly, B. C., et al. 2010, *ApJ*, 719, 1315  
Kim, M., Ho, L. C., Peng, C. Y., Barth, A. J., & Im, M. 2008, *ApJS*, 179, 283  
King, A. 2003, *ApJ*, 596, L27  
Kollatschny, W. 2003, *A&A*, 407, 461  
Kollatschny, W., & Zetzl, M. 2011, *Nature*, 470, 366  
Kollatschny, W., & Zetzl, M. 2013, *A&A*, 549, 100

- Kollmeier, J. A., et al. 2006, *ApJ*, 648, 128
- Konigl, A., & Kartje, J. F. 1994, *ApJ*, 434, 446
- Koratkar, A., & Blaes, O. 1999, *PASP*, 111, 1
- Kormendy, J., & Ho, L. C. 2013, *ARA&A*, in press
- Kormendy, J., & Richstone, D. 1995, *ARA&A*, 33, 581
- Kozłowski, S., et al. 2010, *ApJ*, 708, 927
- Krolik, J. H. 1999, *Active Galactic Nuclei: from the central black hole to the galactic environment*, Princeton University Press
- Krolik, J. H. 2001, *ApJ*, 551, 72
- Kurk, J. D., et al., 2007, *ApJ*, 669, 32
- La Mura, G., Di Mille, F., Ciroi, S., Popović, L. Č., & Rafanelli, P. 2009, *ApJ*, 693, 1437
- Labita, M., Decarli, R., Treves, A., & Falomo, R. 2009a, *MNRAS*, 396, 1537
- Labita, M., Decarli, R., Treves, A., & Falomo, R. 2009b, *MNRAS*, 399, 2099
- Laor, A. 1990, *MNRAS*, 246, 369
- Laor, A. 1998, *ApJ*, 505, L83
- Lauer, T. R., Tremaine, S., Richstone, D., & Faber, S. M. 2007, *ApJ*, 670, 249
- Lawrence, A. 2012, *MNRAS*, 423, 451
- Leighly, K. M. 2004, *ApJ*, 611, 125
- Leighly, K. M., & Moore, J. R. 2004, *ApJ*, 611, 107
- Lewis, G. F., Irwin, M. J., Hewett, P. C., Foltz, C. B. 1998, *MNRAS*, 295, 573
- Li, Y., et al. 2007, *ApJ*, 665, 187
- Lynden-Bell, D. 1969, *Nature*, 223, 690
- Lynden-Bell, D., et al. 1988, *ApJ*, 326, 19
- Lyutyj, V. M., & Cherepashchuk, A. M. 1974, *Astronomicheskii Tsirkulyar*, 831, 1
- McHardy, I. M., Koending, E., Knigge, C., Uttley, P., & Fender, R. P. 2006, *Nature*, 444, 730
- MacLeod, C. L., et al. 2010, *ApJ*, 721, 1014
- MacLeod, C. L., et al. 2012, *ApJ*, 753, 106
- Malkan, M. A. 1983, *ApJ*, 268, 582
- Malmquist, K. G. 1922, *Lund Medd. Ser. I*, 100, 1
- Marconi, A., & Hunt, L. K. 2003, *ApJ*, 589, L21
- Marconi, A., et al. 2004, *MNRAS*, 351, 169
- Marconi, A., et al. 2008, *ApJ*, 678, 693
- Marconi, A., et al. 2009, *ApJ*, 698, L103
- Marziani, P., & Sulentic, J. W. 2012, *NewAR*, 56, 49
- Marziani, P., Sulentic, J. W., Stirpe, G. M., Zamfir, S., & Calvani, M. 2009, *A&A*, 495, 83
- Marziani, P., Sulentic, J. W., Plauchu-Frayn, I., & del Olmo, A. 2013, arXiv:1301.0520
- Matsuoka, K., et al. 2013, *ApJ*, submitted, arXiv:1301.2332
- McConnell, N. J., & Ma, C.-P. 2012, *ApJ*, in press, arXiv:1211.2816
- McGill, K. L., Woo, J., Treu, T., & Malkan, M. A. 2008, *ApJ*, 673, 703
- McLeod, K. K., & Bechtold, J. 2009, *ApJ*, 704, 415
- McLure, R. J., & Dunlop, J. S. 2004, *MNRAS*, 352, 1390
- McLure, R. J., & Jarvis, M. J. 2002, *MNRAS*, 337, 109
- Merloni, A., et al. 2010, *ApJ*, 708, 137
- Metzroth, K. G., Onken, C. A., & Peterson, B. M. 2006, *ApJ*, 647, 901

- Morgan, C. W., Kochanek, C. S., Morgan, N. D., & Falco, E. E. 2010, *ApJ*, 712, 1129
- Mortlock, D. J., et al. 2011, *Nature*, 474, 616
- Mosquera, A. M., & Kochanek, C. S. 2011, *ApJ*, 738, 96
- Murray, N., Chiang, J., Grossman, S. A., & Voit, G. M. 1995, *ApJ*, 451, 498
- Netzer, H. 1990, in *Active Galactic Nuclei*, ed. T. J.-L. Courvoisier & M. Mayor, 137
- Netzer, H. 2009, *ApJ*, 695, 793
- Netzer, H., & Laor, A. 1993, *ApJ*, 404, L51
- Netzer, H., Lira, P., Trakhtenbrot, B., Shemmer, O., & Cury, I. 2007, *ApJ*, 671, 1256
- Netzer, H., & Marziani, P. 2010, *ApJ*, 724, 318
- Netzer, H., & Peterson, B. M. 1997, *Astrophysics and Space Science Library*, 218, 85
- Netzer, H., & Trakhtenbrot, B. 2007, *ApJ*, 654, 754
- Nobuta, K., et al. 2012, *ApJ*, 761, 143
- O'Neill, P. M., Nandra, K., Papadakis, I. E., & Turner, T. J. 2005, *MNRAS*, 358, 1405
- Omukai, K., Schneider, R., & Haiman, Z. 2008, *ApJ*, 686, 801
- Onken, C. A., et al. 2007, *ApJ*, 670, 105
- Onken, C. A., et al. 2004, *ApJ*, 615, 645
- Onken, C. A., & Kollmeier, J. A. 2008, *ApJ*, 689, L13
- Onken, C. A., & Peterson, B. M. 2002, *ApJ*, 572, 746
- Pancoast, A., et al. 2012, *ApJ*, 754, 49
- Papadakis, I. E. 2004, *MNRAS*, 348, 207
- Park, D., et al. 2012a, *ApJ*, 747, 30
- Park, D., Kelly, B. C., Woo, J. H., & Treu, T. 2012b, *ApJS*, 203, 6
- Pelupessy, F. I., Di Matteo, T., & Ciardi, B. 2007, *ApJ*, 665, 107
- Peng, C. Y., Impey, C. D., Ho, L. C., Barton, E. J., & Rix, H.-W. 2006a, *ApJ*, 640, 114
- Peng, C. Y., et al. 2006b, *ApJ*, 649, 616
- Peng, C. Y. 2007, *ApJ*, 671, 1098
- Peterson, B. M. 1993, *PASP*, 105, 247
- Peterson, B. M. 1997, *An Introduction to Active Galactic Nuclei*, ed. B. M. Peterson
- Peterson, B. M. 2010, *IAU Symposium*, 267, 151
- Peterson, B. M. 2011, in *Narrow-Line Seyfert 1 Galaxies and their Place in the Universe*, *Proceedings of Science*, vol. NLS1, 32
- Peterson, B. M., & Wandel, A. 1999, *ApJ*, 521, L95
- Peterson, B. M., & Wandel, A. 2000, *ApJ*, 540, L13
- Peterson, B. M., et al. 2002, *ApJ*, 581, 197
- Peterson, B. M., et al. 2004, *ApJ*, 613, 682
- Popović, L. Č, Mediavilla, E. G., & Muñoz, J. A. 2001, *A&A*, 378, 295
- Portinari, L., Kotilainen, J., Falomo, R., & Decarli, R. 2012, *MNRAS*, 420, 732
- Proga, D., Stone, J. M., & Kallman, T. R. 2000, *ApJ*, 543, 686
- Rafiee, A., & Hall, P. B. 2011a, *MNRAS*, 825
- Rafiee, A., & Hall, P. B. 2011b, *ApJS*, 194, 42
- Richards, G. T., et al. 2002, *AJ*, 124, 1
- Richards, G. T., et al. 2004a, *ApJ*, 610, 679
- Richards, G. T., et al. 2004b, *AJ*, 127, 1305
- Richards, G. T., et al. 2006a, *AJ*, 131, 2766

- Richards, G. T., et al. 2006b, *AJ*, 131, 49  
Richards, G. T., et al. 2011, *AJ*, 141, 167  
Risaliti, G., & Elvis, M. 2010, *A&A*, 516, 89  
Robertson, B., et al. 2006, *ApJ*, 641, 90  
Rokaki, E., Boisson, C., & Collin-Souffrin, S. 1992, *A&A*, 253, 57  
Runnoe, J. C., et al. 2013, *MNRAS*, 429, 135  
Salpeter, E. E. 1964, *ApJ*, 140, 796  
Salucci, P., Szuszkiewicz, E., Monaco, P., & Danese, L. 1999, *MNRAS*, 307, 637  
Salviander, S., Shields, G. A., Gebhardt, K., & Bonning, E. W. 2007, *ApJ*, 662, 131  
Salviander, S., & Shields, G. A. 2012, arXiv:1210.7263  
Schmidt, M. 1963, *Nature*, 197, 1040  
Schneider, P., Ehlers, J., & Falco, E. E. 1992, *Gravitational Lenses*  
Schneider, D. P., et al. 2010, *AJ*, 139, 2360  
Schulze, A., & Wisotzki, L. 2010, *A&A*, 516, 87  
Schulze, A., & Wisotzki, L. 2011, *A&A*, 535, 87  
Sesar, B., et al. 2007, *AJ*, 134, 2236  
Shakura, N. I., & Sunyaev, R. A. 1973, *A&A*, 24, 337  
Shankar, F. 2009, *NewAR*, 53, 57  
Shankar, F., Bernardi, M., & Haiman, Z. 2009, *ApJ*, 694, 867  
Shankar, F., Salucci, P., Granato, G. L., De Zotti, G., & Danese, L. 2004, *MNRAS*, 354, 1020  
Shemmer, O., et al. 2004, *ApJ*, 614, 547  
Shen, J., Vanden Berk, D. E., Schneider, D. P., & Hall, P. B. 2008b, *AJ*, 135, 928  
Shen, Y., Greene, J. E., Strauss, M. A., Richards, G. T., & Schneider, D. P. 2008a, *ApJ*, 680, 169  
Shen, Y., & Kelly, B. C. 2010, *ApJ*, 713, 41  
Shen, Y., & Kelly, B. C. 2012, *ApJ*, 746, 169  
Shen, Y., & Liu, X. 2012, *ApJ*, 753, 125  
Shen, Y., et al. 2011, *ApJS*, 194, 45  
Shibata, M., & Shapiro, S. L. 2002, *ApJ*, 572, L39  
Shields, G. A. 1978, *Nature*, 272, 706  
Shields, G. A., et al. 2003, *ApJ*, 583, 124  
Shields, G. A., Menezes, K. L., Massart, C. A., & Vanden Bout, P. 2006, *ApJ*, 641, 683  
Silk, J., & Rees, M. J. 1998, *A&A*, 331, L1  
Simmons, B. D., & Urry, C. M. 2008, *ApJ*, 683, 644  
Sluse, D., et al. 2011, *A&A*, 528, 100  
Sluse, D., Hutsemékers, D., Courbin, F., Meylan, G., & Wambsganss, J. 2012, *A&A*, 544, 62  
Softan, A. 1982, *MNRAS*, 200, 115  
Stacy, A., Greif, T. H., & Bromm, V. 2012, *MNRAS*, 422, 290  
Steinhardt, C. L., & Elvis, M. 2010a, *MNRAS*, 402, 2637  
Steinhardt, C. L., & Elvis, M. 2010b, *MNRAS*, 406, L1  
Steinhardt, C. L., Elvis, M., & Amarie, M. 2011, *MNRAS*, 415, 732  
Steinhardt, C. L., & Elvis, M. 2011, *MNRAS*, 410, 201  
Sulentic, J. W., Bachev, R., Marziani, P., Negrete, C. A., & Dultzin, D. 2007, *ApJ*, 666, 757  
Sulentic, J. W., Marziani, P., & Dultzin-Hacyan, D. 2000b, *ARA&A*, 38, 521  
Sulentic, J. W., et al. 2002, *ApJ*, 566, L71

- Sulentic, J. W., Zwitter, T., Marziani, P., & Dultzin-Hacyan, D. 2000a, *ApJ*, 536, L5
- Sun, W.-H., & Malkan, M. A. 1989, *ApJ*, 346, 68
- Tanaka, T., & Haiman, Z. 2009, *ApJ*, 696, 1798
- Targett, T. A., Dunlop, J. S., & McLure, R. J. 2012, *MNRAS*, 420, 3621
- Trakhtenbrot, B., & Netzer, H. 2012, *MNRAS*, 427, 3081
- Trakhtenbrot, B., Netzer, H., Lira, P., Shemmer, O. 2011, *ApJ*, 730, 7
- Tremaine, S., et al. 2002, *ApJ*, 574, 740
- Treu, T., Malkan, M. A., & Blandford, R. D. 2004, *ApJ*, 615, L97
- Treu, T., Woo, J.-H., Malkan, M. A., & Blandford, R. D. 2007, *ApJ*, 667, 117
- Tripp, T. M., Bechtold, J., Green, R. F. 1994, *ApJ*, 433, 533
- Trump, J. R., et al. 2009, *ApJ*, 700, 49
- Tsuzuki, Y., Kawara, K., Yoshii, Y., Oyabu, S., Tanabé, T., & Matsuoka, Y. 2006, *ApJ*, 650, 57
- Turk, M. J., Abel, T., & O'Shea, B. 2009, *Science*, 325, 601
- Turner, E. L. 1991, *AJ*, 101, 5
- Tytler, D., & Fan, X.-M. 1992, *ApJS*, 79, 1
- Vanden Berk, D. E., et al. 2004, *ApJ*, 601, 692
- Vestergaard, M. 2002, *ApJ*, 571, 733
- Vestergaard, M. 2004, *ApJ*, 601, 676
- Vestergaard, M., et al. 2011, in *Narrow-Line Seyfert 1 Galaxies and their Place in the Universe*, Proceedings of Science, vol. NLS1, 38
- Vestergaard, M., Fan, X., Tremonti, C. A., Osmer, P. S., & Richards, G. T. 2008, *ApJ*, 674, L1
- Vestergaard, M., & Osmer, P. S. 2009, *ApJ*, 699, 800
- Vestergaard, M., & Peterson, B. M. 2006, *ApJ*, 641, 689
- Vestergaard, M., & Wilkes, B. J. 2001, *ApJS*, 134, 1
- Volonteri, M. 2010, *A&A Review*, 18, 279
- Volonteri, M., & Rees, M. J. 2005, *ApJ*, 633, 624
- Walter, F., et al. 2004, *ApJ*, 615, L17
- Wandel, A., & Yahil, A. 1985, *ApJ*, 295, L1
- Wandel, A., & Petrosian, V. 1988, *ApJ*, 329, L11
- Wandel, A., Peterson, B. M., & Malkan, M. A. 1999, *ApJ*, 526, 579
- Wang, H., et al. 2011, *ApJ*, 738, 85
- Wang, J., et al. 2009, *ApJ*, 707, 1334
- Wang, R., et al. 2010, *ApJ*, 714, 699
- Wang, T., Brinkmann, W., & Bergeron, J. 1996, *A&A*, 309, 81
- Watson, D., Denney, K. D., Vestergaard, M., & Davis, T. M. 2011, *ApJ*, 740, L49
- Wilhite, B. C., Brunner, R. J., Schneider, D. P., & Vanden Berk, D. E. 2007, *ApJ*, 669, 791
- Willott, C. J., et al., 2010, *AJ*, 140, 546
- Wills, B. J., & Browne, I. W. A. 1986, *ApJ*, 302, 56
- Woltjer, L. 1959, *ApJ*, 130, 38
- Woo, J.-H., Treu, T., Malkan, M. A., & Blandford, R. D. 2006, *ApJ*, 645, 900
- Woo, J.-H., Treu, T., Malkan, M. A., & Blandford, R. D. 2008, *ApJ*, 681, 925
- Woo, J.-H. 2008, *AJ*, 135, 1849
- Woo, J.-H., & Urry, C. M. 2002, *ApJ*, 579, 530
- Woo, J.-H., et al. 2010, *ApJ*, 716, 269



- Wu, X.-B., Wang, R., Kong, M. Z., Liu, F. K., & Han, J. L. 2004, *A&A*, 424, 793
- Wyithe, J. S. B., & Loeb, A. 2002, *Nature*, 417, 923
- Wyithe, J. S. B., & Loeb, A. 2012, *MNRAS*, 425, 2892
- Xiao, T., et al. 2011, *ApJ*, 739, 28
- Yoo, J., & Miralda-Escudé, J. 2004, *ApJ*, 614, L25
- Yu, Q., & Tremaine, S. 2002, *MNRAS*, 335, 965
- Zhang, X., Lu, Y., & Yu, Q. 2012, *ApJ*, 761, 5
- Zhou, X.-L., Zhang, S.-N., Wang, D.-X., & Zhu, L. 2010, *ApJ*, 710, 16
- Zel'dovich, Y. B., & Novikov, I. D. 1964, *Dokl. Akad. Nauk SSSR*, 158, 811
- Zu, Y., Kochanek, C. S., & Peterson, B. M. 2011, *ApJ*, 735, 80